The Holocene 16,7 (2006) pp. 949–965

Rapid sea-level rise in the North Atlantic Ocean since the first half of the nineteenth century

W. Roland Gehrels,[1]* William A. Marshall,[1] Maria J. Gehrels,[1] Gudrún Larsen,[2] Jason R. Kirby,[3] Jón Eiríksson,[2] Jan Heinemeier[4] and Tracy Shimmield[5]

([1]School of Geography, University of Plymouth, Plymouth PL4 8AA, UK; [2]Science Institute, University of Iceland, Reykjavik, Iceland; [3]School of Biological and Earth Sciences, John Moores University, Liverpool L3 3AF, UK; [4]Department of Physics and Astronomy, University of Aarhus, DK-8000 Aarhus C, Denmark; [5]Dunstaffnage Marine Laboratory, Oban PA34 4AD, UK)

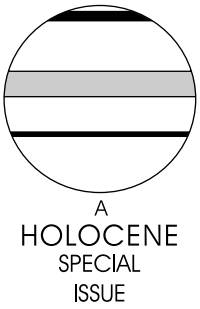

Abstract: A high-resolution late-Holocene sea-level record is produced from salt-marsh deposits at Viðarhólmi in Snæfellsnes, western Iceland. The stratigraphy of Viðarhólmi saltmarsh is documented using detailed descriptions of ten exposed sections and numerous hand-drilled cores. Fossil foraminifera are used as proxy sea-level indicators in an exposed section of salt-marsh peat. The agglutinated foraminifera *Jadammina macrescens* and *Paratrochammina* (Lepidoparatrochammina) *haynesi* are most useful as sea-level indicators because of their narrow vertical extent on the marsh surface and their good preservation in the peaty marsh deposits. We collected compaction-free sea-level index points from salt-marsh peat directly overlying the bedrock surface to establish the pre-industrial millennial-scale trend of sea-level rise and evaluate effects of autocompaction on the stratigraphy. The chronology of the sea-level reconstruction is based on tephra stratigraphy, AMS ^{14}C, ^{137}Cs, Pb and palaeomagnetic analyses. The main tephra layer visible in the stratigraphy of Viðarhólmi salt marsh is the Landnám (settlement) layer, previously dated to AD 875±6. A sea-transported pumice layer was correlated to the 'Mediaeval Layer' of AD 1226/27. Our reconstruction indicates that relative sea level along the coast of western Iceland has risen by about 1.3 m since *c.* AD 100. The detrended sea-level record shows a slow rise between AD 100 and 500, followed by a slow downward trend reaching a lowstand in the first half of the nineteenth century. This falling trend is consistent with a steric change estimated from reconstructions of sea-surface and sea-bottom temperatures from shelf sediments off Northern Iceland. The sea-level record shows a marked recent rise of about 0.4 m that commenced AD 1820±20 as dated by palaeomagnetism and Pb produced by European coal burning. This rapid sea-level rise is interpreted to be related to global temperature rise. The rise has continued up to the present day and has also been measured, since 1957, by the Reykjavik tide gauge.

Key words: Dating, Iceland, late Holocene, saltmarsh, sea-level change, tephra, HOLSMEER project.

Introduction

Sea-level observations from satellites have shown an acceleration of global sea-level rise in the past decade compared with the previous 50 years (Cazenave and Nerem, 2004), but evidence of a twentieth-century acceleration compared with the nineteenth century has been disputed. In a recent study, Church and White (2006) report signs of a global sea-level acceleration around 1930. Their data base, however, contained only ten instrumental records of sea-level observations from the 1870s and, perhaps unsurprisingly, earlier investigations of the same long tide-gauge records failed to find evidence of a twentieth-century sea-level acceleration (Woodworth, 1990; Douglas, 1992). Studies based on geological proxies in the western Atlantic Ocean have documented this acceleration much more clearly (Donnelly *et al.*, 2004; Gehrels *et al.*, 2005). High-resolution proxy methods have the advantage that the sea-level record can be extended back in time beyond the range of instrumental records whilst the proxy record for the twentieth century can be directly compared with tide-gauge records to validate the method of reconstruction (Gehrels, 2000).

*Author for correspondence (e-mail: wrgehrels@plymouth.ac.uk)

10.1177/0959683606hl986rp

This paper reports on a recent acceleration of sea-level rise along the coast of western Iceland reconstructed by proxy data collected from salt-marsh sediments. This part of the northern Atlantic Ocean is poorly covered by instrumental sea-level observations. The Reykjavik tide-gauge record commenced in 1957 and shows a rate of rise of 2.3 ± 0.5 mm/yr (Woodworth and Player, 2003; Permanent Service for Mean Sea Level (PSMSL), 2004). From an oceanographic point of view this area is of interest because Iceland's west coast is directly exposed to the Irminger Current, an important branch of the North Atlantic oceanic circulation. Several recent studies have produced high-resolution late-Holocene palaeoceanographic records from the Icelandic shelves (eg, Jennings *et al.*, 2001; Andrews and Giraudeau, 2003; Andrews *et al.*, 2003; Knudsen *et al.*, 2004). The study by Knudsen *et al.* (2004) is of particular relevance as it provides a palaeoenvironmental record of sea-surface and sea-bottom temperatures during the past 1200 years. When compared with such records, a high-resolution relative sea-level record from coastal Iceland offers the opportunity to evaluate the influence of oceanographic changes as a driver of sea-level change. The incorporation of sea-level changes into ocean circulation models is an emerging area of interest in sea-level studies (Crowley *et al.*, 2003; van de Plassche *et al.*, 2003; van der Schrier *et al.*, 2004).

Traditionally, data on relative sea-level changes in Iceland have provided information on vertical isostatic land movements related to Iceland's deglaciation history (Thors and Boulton, 1991; Thors and Helgadóttir 1991; Sveinbjornsdottir *et al.*, 1993; Ingólfsson *et al.*, 1995; Rundgren *et al.*, 1997; Ingólfsson and Norddahl, 2001; Norddahl and Einarsson, 2001; Norddahl and Petursson, 2005). In the Reykjavik area, for example, a rapid postglacial sea-level fall has been documented between *c.* 10 300 and 9500 ^{14}C yr BP from a highstand at 65 m above present sea level to a lowstand 30–35 m below present sea level (Thors and Helgadóttir, 1991). The Holocene sea-level history, however, is poorly constrained in western Iceland. Limited evidence comes from Iceland's northwest peninsula where several Holocene shorelines are found between 0 and 10 m above present sea level (Hansom and Briggs, 1991). This suggests that differential isostatic movements have played an important role in shaping western Iceland's coastal environments. Isostatic rebound is continuing in modern times, possibly as a result of recent volume changes of ice caps, the largest of which is the Vatnajokull (Sjoberg *et al.*, 2000). Nonetheless, late-Holocene relative sea-level data in Iceland are sparse and only recently have Simonarson and Leifsdóttir, (2002) reported sea-level data from a stretch of coastline in southern Iceland (Flói) that is seismically active but where they argued that volcanically induced crustal subsidence could be discounted. They documented a 2 m rise in sea level between 3200 and 2200 cal. yr BP, followed by a 3 m drop around 2000 cal. yr BP. This record, however, only contains four sea-level index points and is therefore of limited value for a high-resolution study.

Study area

In this paper we establish a high-resolution late-Holocene sea-level record from saltmarsh deposits at Viðarhólmi in Snæfellsnes, western Iceland (Figure 1). The salt marsh at Viðarhólmi (Icelandic for 'wooded island') is the largest saltmarsh in Iceland (Ingólfsson, 1994). An alternative name for the marsh, used in the literature, is Melabakkar (Ingólfsson, 1994, Skirnisson *et al.*, 2004). The marsh forms part of an extensive area of salt marsh in the northeastern

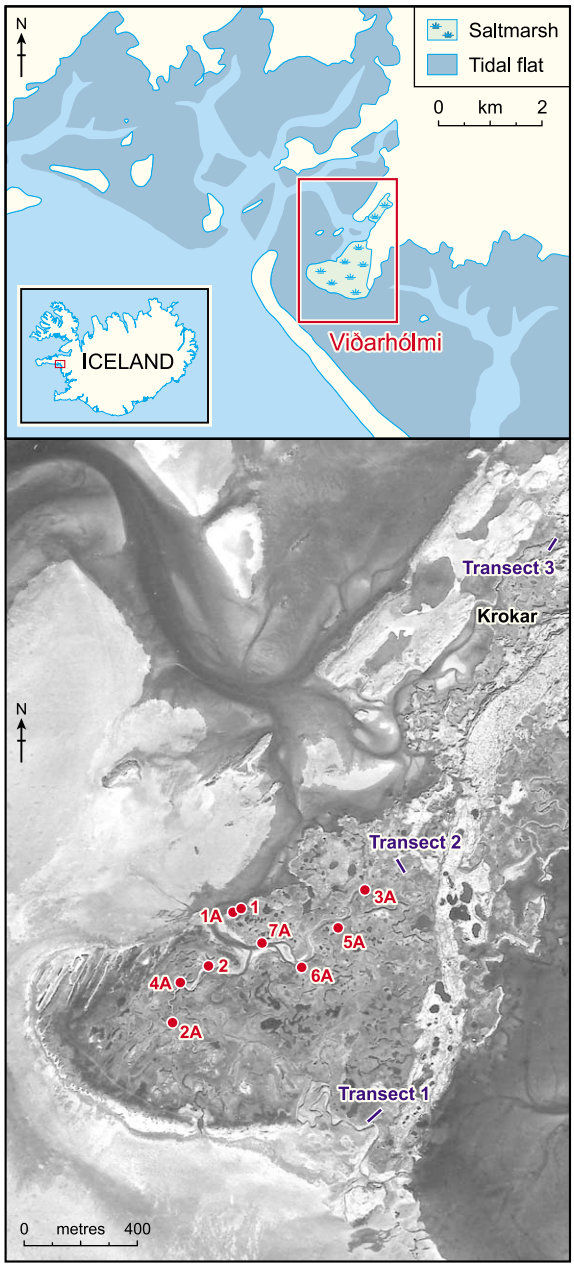

Figure 1 Location map, showing the locations of nine logged sections (Figure 2), two transects (1 and 2) sampled for surface foraminifera, and one transect (3) in the Krokar marsh sampled for basal peat (Figure 2)

corner of Faxaflói Bay, a meso- to macrotidal embayment between the Reykjanes peninsula to the south and the Snæfellsnes peninsula to the north. Here, salt marshes are well developed and exhibit a clear plant zonation related to tidal flooding. The dominant plants in the upper part of the intertidal zone are *Carex lyngbyei*, *Agrostis stolonifera*, *Festuca rubra* and *Puccinellia maritima* (Ingólfsson, 1998). As a result of meandering of tidal creeks, the stratigraphy of the salt marsh is exposed along continuous vertical sections. The marsh is virtually untouched by human activities, although some sheep occasionally graze in its upper portions.

Our study area is located in a part of western Iceland that is seismically inactive (Angelier *et al.*, 2004). The bedrock basement in the area consists of Tertiary basalts. The salt marsh is surrounded by volcanic lava flows that are Holocene in age and at least 5000 years old. They were produced by an eruption of the Eldborg crater (Thordarson and Höskuldsson, 2002). Interestingly, a volcanic eruption that occurred in this area

around AD 900 is mentioned in Iceland's Book of Settlement. By mapping ash isopachs in a confined area to the east of the marsh, Jóhannesson (1977) determined that this eruption originated from the nearby Raudhalsar volcano.

Methods

Fieldwork in Iceland was conducted in July 2001 and September 2003. The stratigraphy of the salt marsh was established based on hand coring and logging of exposed sections along tidal creek banks. We sampled one representative exposure (section 3A) with monolith tins in 2001. Section 3A was selected on the basis of its position in the high marsh, well away from the tidal flats. It provided a uniform and undisturbed peat sequence with two visible tephra horizons (see below). In 2003 the exposure was re-visited and more material was collected.

Subsamples from the 2001 tins were subjected to foraminiferal analyses at 1–2 cm resolution. Modern foraminifera were sampled in 1 cm thick samples from the surface of the salt marsh along two transects. All foraminifera samples were sieved between 63 and 500 μm and stained with rose Bengal to separate living from dead species. Details of foraminiferal sampling and preparation techniques are described in Gehrels (2002). Heights of all sample sites were surveyed relative to geodetic and tidal datums. From interpolation between tidal stations (Admiralty Tide Tables, 2001) and our survey data we estimate that the mean tidal range at Viðarhólmi is 2.1 m and that mean sea level is 0.12 m above the Iceland geodetic datum. The highest astronomical tides are estimated to reach ~2.1 m above MSL at Viðarhólmi.

From the data set of dead surface foraminifera we constructed a transfer function using the software C^2 (Juggins, 2003) to quantify the relationship between height and the foraminiferal assemblages. The transfer function was applied to the foraminiferal stratigraphy of section 3A to produce a record of saltmarsh surface height changes. This record was combined with a detailed age–depth model to produce a late-Holocene relative sea-level history for western Iceland.

We used a variety of methods to derive the age–depth model for the section. The chronology before *c.* AD 1700 is based on AMS ^{14}C and tephra analyses in the 2001 monoliths. The minerogenic nature of the saltmarsh sediments and the abundance of locally derived and weathered glass shards necessitated a somewhat tiresome sample preparation procedure for tephra analyses. Samples were taken at 0.5 cm intervals and burnt at 500°C for 3 h to remove organic material and determine loss-on-ignition (LOI) values. Hydrochloric acid (10%) was added to the ash and the mixture warmed to aid dispersion. Standardized concentration tablets of *Lycopodium* spores were added and the liquid centrifuged off. The remaining solid material was dried at 50°C, cooled, and suspended in 500 μL of glycerol. Subsamples of this suspension were mounted on glass slides, and the tephra shards identified using a polarizing microcope at 400× magnification. Unweathered brown (basaltic) and clear (rhyolotic) shards were counted alongside *Lycopodium* spores to determine shard concentrations for each sample (Gehrels *et al.*, 2006). Guided by these results, nine sediment samples were prepared for microprobe analysis using the acid digestion method (Dugmore, 1989) to remove the organic component. This method does not appreciably alter the geochemistry of the glass (Dugmore *et al.*, 1992). After drying at 50°C, unweathered shards were separated by hand, using a fine paint brush under low power microscope and mounted on preground glass slides using EPO-TEH 301 (Epoxy Technology Inc.) epoxy resin. Once hardened, the resin was ground flat and polished with Kemet diamond paste (1 μm) to expose the glass shards.

Microprobe analyses to identify tephra sources were performed by standard wavelength dispersal technique on an ARL-SEMQ microprobe at the Geological Institute, University of Bergen, Norway, with an accelerating voltage of 15 kV, a beam current of 10 nA and a defocused beam diameter of 6–12 μm. Natural and synthetic minerals and glasses were used as standards. Sediment that was microprobed included nine samples from our 'master' section 3A and six samples from section 1.

AMS ^{14}C analyses were conducted at the tandem accelerator in the University of Aarhus AMS Dating Centre. We selected fragile, horizontally embedded, detrital plant fragments for dating. The choice of this type of dating material maximizes the possibility that dated samples are contemporaneous with the former marsh surface on which they were deposited. Radiocarbon ages were calibrated using the INTCAL04 calibration curve (Reimer *et al.*, 2004).

The youngest sediments were dated using a combination of ^{210}Pb, ^{137}Cs, total Pb and Li concentrations, Pb isotopic ratios and palaeomagnetic analyses. Radio-isotopes of Pb and Cs were measured in the 2001 monoliths from dried material by gamma spectroscopy using a Canberra low-energy Germanium detector at the Dunnstaffnage Laboratory of the Scottish Marine Association in Oban, UK. Total Pb and Li concentrations and stable Pb isotopic ratios were measured in the 2003 monoliths at the University of Plymouth using an ICP-MS PlasmaQuad PQ2+ Turbo and an Axiom Multicollector ICP-MS PlasmaQuad PQ2+ Turbo, respectively. Past changes in magnetic declination in the 2003 monoliths were measured at the Southampton Oceanographic Centre using a 2-G Enterprises cryogenic magnetometer.

Results

Lithostratigraphy

The stratigraphy of Viðarhólmi salt marsh was logged in nine exposed vertical sections along the main tidal channel (Figure 2A). The salt marsh sediments of Viðarhólmi are peaty, but also contain interbedded thin layers of well-sorted, black volcanic sands. These sands are most likely of aeolian origin, blown in from surrounding intertidal and upland areas where sands are abundantly available. They may also represent overwash events, but this could not be firmly established given the absence of allochthonous foraminifera in the sand. Two important markers in the stratigraphy are a coarse sea-transported pumice layer, between 1.2 and 1.4 m above MSL, and a visible white tephra layer, between 0.8 and 1.1 m above MSL. At the bottom of some of the sections, between 0.5 and 0.8 m above MSL, another pumice layer is found.

Cores were collected along a transect in the Krokar marsh (Figure 1). Here, the upper pumice layer could be traced to where it lies on bedrock, at 1.5 m above MSL (Figure 2B). In contrast to the exposed sections, the thin tephra layer could not be visually detected in the cores because of the smeared nature of the sediment. From the base of three cores we collected basal peat samples that were dated to provide compaction-free sea-level index points.

Biostratigraphy

Foraminiferal analyses show that the stratigraphy in section 3A consists almost entirely of upper salt-marsh facies (Figure 3). This is important, as the upper salt marsh is the part of the

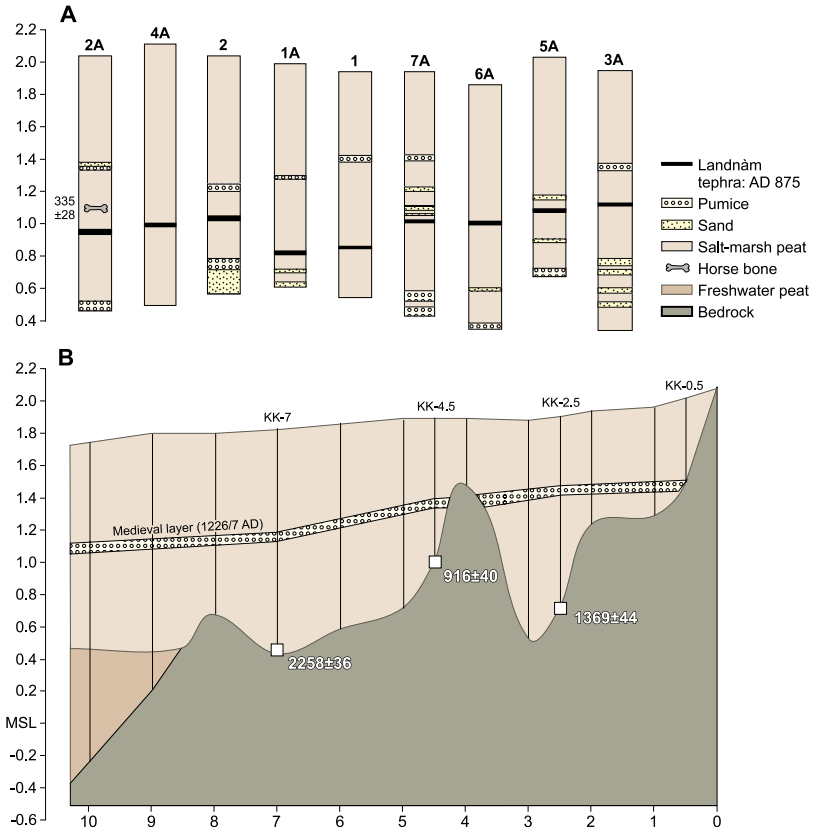

Figure 2 Stratigraphy of nine logged sections (A) and Krokar transect 3 (B). The horse bone in section 2 was radiocarbon dated to 335±28 (AAR-7226). The Krokar section provides four basal sea-level index points, three from radiocarbon ages in cores KK-2.5, KK-4.5 and KK-7 and one from the pumice layer in core KK-0.5. See Figure 3 for radiocarbon dates in section 3A

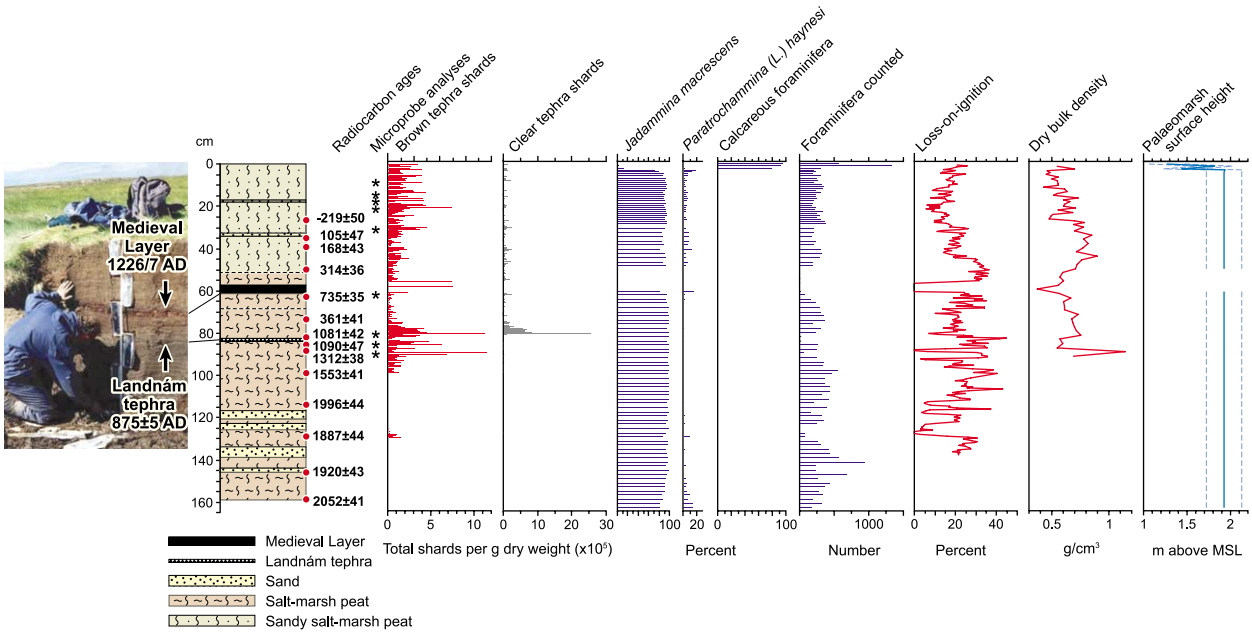

Figure 3 Stratigraphy of section 3A, shown with radiocarbon chronology, tephra shard counts, foraminiferal analyses, loss-on-ignition and dry bulk density. Nine tephra samples (asterisks) were subjected to microprobe analyses. The reconstructed palaeomarsh surface height changes are calculated from regression analyses (see text for explanation)

marsh where sea-level changes are most sensitively recorded (Allen, 1990). The sequence is dominated by *Jadammina macrescens*, a typical high marsh foraminifer (Gehrels and van de Plassche, 1999). The only other agglutinated foraminifer present in the stratigraphy is *Paratrochammina* (Lepidoparatrochammina) *haynesi*. This species has been found in the high salt marshes in Ho Bugt, western Denmark (Gehrels and Newman, 2004). Calcareous foraminifera occur in the top 3 cm of the section, but these are likely to have been deposited as a result of recent tidal creek overwash. From the shallow presence of these foraminifera it is inferred that the cutting of the creek bank along which the section is exposed is a recent phenomenon. The top three samples are not used in our sea-level reconstruction.

AMS ^{14}C

From section 3A we obtained 13 AMS ^{14}C ages on detrital plant fragments (Table 1). All ages are in stratigraphic order, with the exception of AAR-8035 (361 ± 41 ^{14}C yr BP), which was excluded from our age–depth model. One other sample (AAR-8030) returned a modern age and was also excluded.

We used a probability modelling approach to determine the age–depth model from the calibrated radiocarbon ages (Figure 4), following Gehrels *et al.* (2005). For each measurement (ie, sample), two sets of age ranges and relative probability for each mode were separated: modes of ±1σ (68% confidence intervals) and modes of ±2σ (95% confidence intervals). All measurements were assigned a weight of 1. The Landnám tephra horizon and the 'Mediaeval Layer' (see next section) were arbitrarily assigned weights of 10 to indicate their superior chronostratigraphic value. Their probability distributions were treated as unimodal. The weighted probabilities of the calibrated ^{14}C ranges were calculated from the relative probability of each 1σ and 2σ age bracket (Reimer *et al.*, 2004) divided by the total probability of each measurement. To ensure that the models provide increasing age with increasing depth we used a weighted moving average algorithm that is applied iteratively over increasing depths until age reversals are

Table 1 Radiocarbon dating results

AAR-	Section	Depth (cm)	Height above MSL (cm)	Weight (mg)	Description	^{14}C age	±	Calibrated age 1σ	δ^{13}C
In-core samples									
8030	3A	27	167	5.2	Detrital plant fragments	−219	50	AD 1955–1956	−27.9
8031	3A	36	158	12.5	Detrital plant fragments	105	47	AD 1681–1952	−27.45
8032	3A	39	155	6.2	Detrital plant fragments	168	43	AD 1665–1949	−28.13
8033	3A	51	143	8.4	Detrital plant fragment	314	36	AD 1495–1643	−26.74
8034	3A	63	131	13.9	Detrital plant material	735	35	AD 1267–1291	−25.26
8035	3A	74	120	20.9	Detrital brown-red (woody) material	361	41	AD 1490–1608	−25.43
8036	3A	83	111	7.9	Detrital plant material	1081	42	AD 898–1015	−28.01
8037	3A	86	108	10.8	Plant fragment	1090	47	AD 894–1000	−28.19
8038	3A	88	106	68.3	Woody (ribbed) piece of *T. maritima* (?)	1312	38	AD 663–767	−25.13
8039	3A	99	95	77	Coarse fragment of *T. maritima* (?)	1553	41	AD 431–559	−24.31
8040	3A	113	81	19.1	*T. maritima* (?) fragment	1696	44	AD 259–413	−25.45
8041	3A	129	65	10.6	(Woody) plant fragment	1887	44	AD 73–208	−24.81
8042	3A	145	49	17.8	Detrital plant material	1920	43	AD 30–128	−25.6
8043	3A	162	32	5.5	Detrital plant fragments	2052	41	108 BC–AD 1	−28.67
7226	2A	92	100	no data	Horse bone (*Equus caballus*)	335	28	AD 1520–1636	−21.74
Basal samples									
8064	KK-2.5	90	101	7.5	Detrital plant fragments	1369	44	AD 644–682	−27.94
8065	KK-4.5	66–67	134–133	9.5	Detrital plant fragments	916	40	AD 1066–1157	−30.04
8066	KK-7	135	48	13	Detrital plant fragment (*Phragmites*?)	2258	36	389–213 BC	−29.33

All samples, except AAR-7226, were dated by AMS.
MSL, mean sea level.

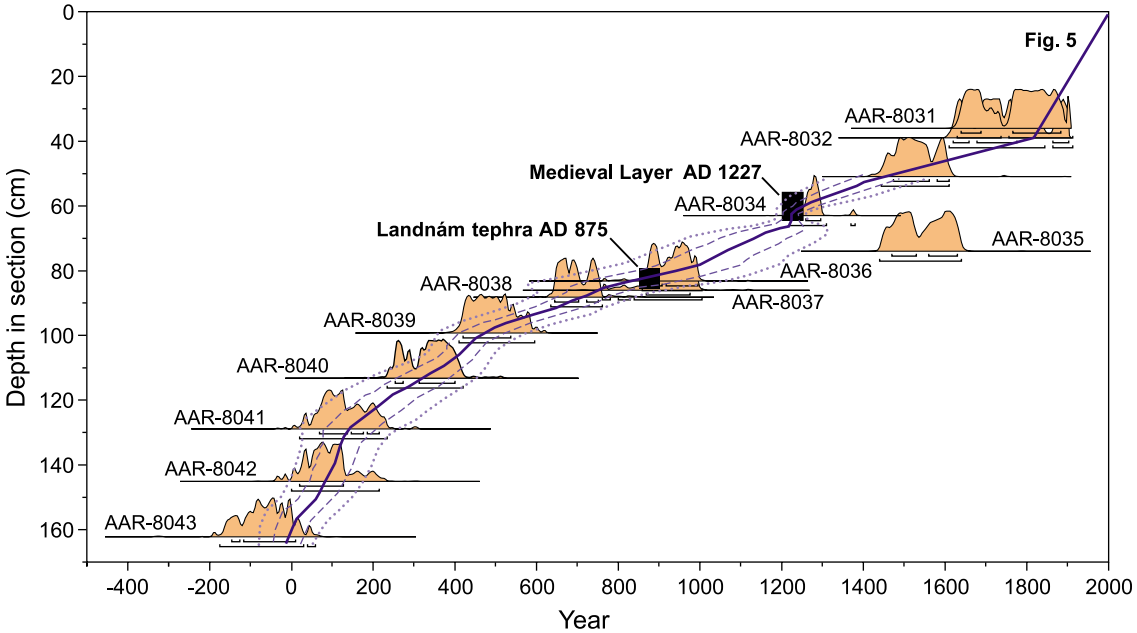

Figure 4 Age model of section 3A based on ^{14}C and tephra analyses. The chronology of the top 55 cm of the section is based on geochemical and magnetic analyses and shown in detail in Figure 5. A Gaussian probability best-fit line was calculated for the tephra and radiocarbon chronology. AAR-8031, AAR-8032 and AAR-8035 were excluded from the age model

removed (in this case 19 cm), allowing age determinations at 1 cm intervals. All mathematical formulae for this probablistic age-modelling approach are reported in Gehrels *et al.* (2005).

In section 2A we encountered a leg bone of a 4- to 5-year old horse (*Equus caballus*, Figure 2A). Horses were introduced into Iceland after Norse settlement, which is in agreement with the age of the bone (335 ± 28 ^{14}C yr BP) and its stratigraphic position above the Landnám (settlement) tephra (see below).

Tephra

The main tephra layer visible in the stratigraphy of Viðarhólmi salt marsh is the Landnám (settlement) layer, dated to the 870s (ie, AD 875 ± 6; Zielinski *et al.*, 1994; Wastegard *et al.*, 2003; Grönvold *et al.*, 1995). Upper and lower contacts of the layer are very sharp and the tephra has not been significantly reworked. Radiocarbon ages above and below the layer are in agreement with the tephra age (Table 2). An extensive sea-transported pumice layer was correlated to the 'Mediaeval Layer' of AD 1226/27 (Table 2), originating from eruptions off the Reykjanes peninsula (Sigurgeirsson, 1992; Haflidason *et al.*, 1992). To determine whether additional tephra horizons were present in the stratigraphy we counted glass shards at 0.5 cm contiguous intervals throughout the top 1 m of section 3A (Figure 3). Promising peaks were subjected to microprobe analysis. We found two possible prehistoric tephra layers, but their ages are not well constrained (Table 2). Unweathered glass shards occur throughout the section. These are mostly of local origin and cannot be tied in with known eruptions (Appendix 1). The lower pumice layer that is visible in the base of some exposed sections was chemically analysed in section 1 (Table 2). Its chemical composition and approximate age (cf. Figure 4) suggest that this pumice layer could have originated from an eruption off the Reykjanes peninsula 1500–2000 years ago (Sigurgeirsson, 1992).

Chronostratigraphic markers in the past 200 years

In the top of the section the radiocarbon ages are of limited use because of the wide age ranges produced by calibration. We therefore rely on a combination of analyses of ^{137}Cs, Pb concentrations, Pb isotopes and palaeomagnetism, providing several useful age markers (Table 3, Figure 5A).

At 39 cm depth we observe an abrupt change in the magnetic declination measurement. We attribute this change to the declination swing between 1800 and 1840 that is documented in the instrumental record of secular variations from the southern UK (Malin and Bullard, 1981; Barraclough *et al.*, 2000; Jackson *et al.*, 2000) and other palaeomagnetic records from the Northern Hemisphere (Jonkers *et al.*, 2003). We use only the declination measurements as the inclination record of the salt-marsh sediments is very noisy. It is also a much more subtle signal that does not provide useful age markers in the past two centuries (Jackson *et al.*, 2000).

At 39 cm depth we also observe a change in Pb concentrations, from low and stable concentrations below 39 cm to fluctuating and slowly rising concentrations higher in the core. In Figure 5A we present this change as standardized against Li to eliminate effects of grain size (Loring, 1991). On the basis of the Pb isotopic ratios, we interpret the change in the Pb profile as the onset of anthropogenic Pb input. The ratios of ^{206}Pb/^{207}Pb and ^{206}Pb/^{208}Pb below 39 cm are similar to those of the Reykjanes volcanic system (Figure 5B), which is also the source of the pumice in the salt marsh (Table 2). In the section between 38 and 14 cm the isotopic Pb ratios change towards those of British coal (Figure 5B). The increase in European Pb emissions, which originated primarily from UK sources (Farmer *et al.*, 1999), has been dated by extrapolation of ^{210}Pb ages to $\sim$1820 in lake sediments from Scotland (Farmer *et al.*, 1999; Eades *et al.*, 2002) and to 1800–1840 in lake sediments in western Greenland (Bindler *et al.*, 2001). In ice core records from the Alps (Schwikowski *et al.*, 2004) and Greenland (Candelone *et al.*, 1995) the Pb increase has been dated by layer counting to 1800–1850. Based on our Pb and magnetic measurements we assign an age of 1820 ± 20 to the level at 39 cm. This age is in agreement with the historical consumption of coal in the UK (Farmer *et al.*, 1999) and represents our best estimate for the timing of a marked increase in the sedimentation rate of the salt marsh (Figure 5A).

Above 39 cm the Pb record contains several markers that can be linked with the history of European Pb emissions. We interpret a dip in Pb concentrations at 16 cm, coinciding with a temporary peak in ^{206}Pb/^{207}Pb ratios, as resulting from stagnating economies during World War I and the subsequent Great Depression (eg, Weiss *et al.*, 1999). The highest Pb concentrations in our record occur at 9 cm depth and have been dated to 1952–1956 in the Faroe Islands (Shotyk *et al.*, 2005), Denmark and Greenland (Shotyk *et al.*, 2003). The Pb peak predominantly reflects the maximum of British coal consumption in the early 1950s (Farmer *et al.*, 1999). The isotopic ratios during the rapid Pb rise between 13 and 9 cm are produced by the increased influence of petrol Pb (Figure 5A, B). The ^{137}Cs peak at 9–10 cm depth (Table 4) is interpreted to result from nuclear bomb testing in 1963, as ^{137}Cs deposition from the Chernobyl accident was minimal in Iceland (Pálsson *et al.*, 1994). This peak overlaps with the Pb maximum and we assign an age of 1960 ± 5 to the level at 9 cm depth. Our inability to distinguish between the Pb and ^{137}Cs maxima may be due partly to some mobility in the ^{137}Cs profile or to a very small offset (< 1 cm) between the 2001 and 2003 monoliths (see Methods section). Changes in Pb concentrations and Pb isotopic ratios in the top of the core (Figure 5A, B) are consistent with the maximum of European petrol consumption around 1980 and the EU ban on leaded petrol in 1987 (Shotyk *et al.*, 2003).

Radiocarbon ages cannot be used to constrain the chronology further in the top 55 cm of our sequence, but we note that our age model is broadly consistent with the two youngest radiocarbon ages at 39 cm (AAR-8032, 168 ± 43) and 36 cm (AAR-8031, 105 ± 47). The median probability calibrated ages for these two dates are AD 1779 and AD 1830, respectively. At the 2σ level, the calibration of AAR-8032 gives a 47.3% probability that the age lies between AD 1718 and AD 1828 and a 15.4% probability that the age lies between AD 1831 and AD 1890. For AAR-8031 there is a 63.7% probability that its age is between AD 1799 and AD 1941 at 2σ (Reimer *et al.*, 2004).

The results of the ^{210}Pb analyses pose some problems (Table 4). Low initial ^{210}Pb activity levels are to be expected as Iceland is naturally depleted in atmospheric ^{210}Pb (Preiss *et al.*, 1996). The unsupported ^{210}Pb activity in the samples is indeed very low ($\sim$50 Bq/kg) and below 12 cm in the section it is below the limit of detection after just 2.5 ^{210}Pb half-lives ($\sim$50 years). This detection problem is further illustrated by the total ^{210}Pb activity below 15 cm of $\sim$8 Bq/kg, significantly lower than the mean ^{226}Ra activity in the deeper part of the section (22 Bq/kg). If ^{210}Pb activities are reliable they should match the ^{226}Ra activity in the older part of the section. In view of these uncertainties we do not include the ^{210}Pb analyses in our age model and base our age estimates only in the younger part of the section on analyses of ^{137}Cs, Pb, Pb isotopic ratios and magnetic declination (Figure 5A). We interpolate between the 1800–1840 age at 39 cm and the AMS^{14}C date at 51 cm,

Table 2 Major element geochemical analyses of volcanic glass shards in sections 1 and 3A. Note that P_2O_5 was analysed in section 1, but not in section 3A. MnO was analysed in section 3A, but not in section 1

SiO_2	TiO_2	Al_2O_3	FeO	MgO	CaO	Na_2O	K_2O	P_2O_5	Sum	Origin
Section 1	*0.58–0.60 m*		*Sea-transported pumice, AD 1226/7*							
50.69	1.84	13.47	13.46	6.71	11.33	2.31	0.13	0.10	100.05	Reykjanes volcanic system (coarse fraction)
50.54	1.74	13.70	13.82	6.67	11.40	2.10	0.17	0.10	100.25	Reykjanes volcanic system (coarse fraction)
50.33	1.73	13.77	13.86	7.09	11.31	1.87	0.21	0.00	100.16	Reykjanes volcanic system (coarse fraction)
49.78	1.72	13.81	13.69	6.83	11.43	2.20	0.16	0.33	99.96	Reykjanes volcanic system (coarse fraction)
49.78	1.79	13.88	13.47	6.53	11.37	2.01	0.10	0.17	99.09	Reykjanes volcanic system (coarse fraction)
49.67	1.89	13.69	13.72	7.23	11.16	1.97	0.23	0.17	99.72	Reykjanes volcanic system (coarse fraction)
50.35	1.92	13.57	13.93	6.35	10.98	2.32	0.22	0.13	99.75	Reykjanes volcanic system (coarse fraction)
50.90	1.74	13.73	13.88	6.46	11.01	2.20	0.23	0.09	100.24	Reykjanes volcanic system (coarse fraction)
48.69	1.68	15.73	10.56	6.78	12.07	2.27	0.69	0.23	98.70	Glass grain of local origin (fine fraction)
49.23	1.58	15.82	10.35	6.68	11.70	2.28	0.69	0.21	98.53	Glass grain of local origin (fine fraction)
66.74	1.00	14.43	5.60	1.06	2.97	3.92	2.76	0.21	98.68	Glass grain of local origin (fine fraction)
59.56	1.50	15.36	7.11	1.63	3.76	4.19	3.12	0.40	96.63	Glass grain of local origin (fine fraction)
54.93	2.01	14.99	12.12	2.95	6.86	3.32	1.20	1.11	99.48	Glass grain of local origin (fine fraction)
Section 1	*1.68–1.70 m*		*Sea-transported pumice, AD 1500–2000*							
50.47	1.82	13.50	14.25	6.31	11.02	1.96	0.17	0.19	99.70	Reykjanes volcanic system (coarse fraction)
50.47	1.82	13.36	13.87	6.36	11.05	2.04	0.25	0.21	99.42	Reykjanes volcanic system (coarse fraction)
50.26	1.94	13.53	14.10	6.43	10.79	2.40	0.19	0.67	100.29	Reykjanes volcanic system (coarse fraction)
49.80	1.80	13.82	13.91	6.68	11.67	2.11	0.24	0.22	100.24	Reykjanes volcanic system (coarse fraction)
48.15	1.84	14.26	13.13	7.43	11.91	1.95	0.20	0.23	99.10	Reykjanes volcanic system (coarse fraction)
Section 3A	*0.63 m*		*Sea-transported pumice, AD 1226/27*							
50.77	1.41	13.71	12.23	0.16	7.10	11.30	2.07	0.11	98.90	Reykjanes volcanic system
49.45	1.85	13.54	12.82	0.22	6.43	11.23	2.23	0.27	98.08	Reykjanes volcanic system
49.32	1.84	13.80	12.56	0.19	6.48	11.11	2.28	0.26	97.86	Reykjanes volcanic system
47.97	1.85	13.33	12.43	0.28	6.34	10.97	2.33	0.24	95.78	Reykjanes volcanic system
70.19	0.29	13.49	3.78	0.11	0.13	1.25	5.11	3.35	97.74	Volc. syst. outside Snæfellsnes
60.82	1.22	16.05	6.48	0.21	1.26	4.38	4.86	2.77	98.09	Glass grain of local origin
46.93	4.29	13.01	14.69	0.23	5.34	9.85	2.76	0.72	97.86	Katla volcanic system
Section 3A	*0.815 m*		*Settlement tephra layer, AD 875 ±6*							
70.79	0.40	14.58	2.34	0.10	0.18	0.90	4.81	4.81	98.96	Settlement tephra, Torfajökull component
70.53	0.90	14.19	2.36	0.08	0.16	0.91	5.02	4.93	99.12	Settlement tephra, Torfajökull component
70.21	0.26	13.85	2.29	0.06	0.15	0.90	4.20	4.47	96.42	Settlement tephra, Torfajökull component
69.93	0.26	14.45	2.23	0.08	0.20	0.86	4.14	4.54	96.73	Settlement tephra, Torfajökull component
69.87	0.15	14.36	2.34	0.09	0.14	0.88	4.37	4.58	96.82	Settlement tephra, Torfajökull component
69.55	0.27	14.39	2.23	0.12	0.15	0.86	4.37	4.57	96.54	Settlement tephra, Torfajökull component
49.31	1.77	13.43	12.93	0.20	6.80	11.70	2.25	0.23	98.66	Settlement tephra, Veidivötn component
49.17	1.88	13.52	12.69	0.20	6.26	11.53	2.15	0.23	97.66	Settlement tephra, Veidivötn component
49.06	1.62	13.35	12.90	0.20	6.65	11.45	2.24	0.20	97.70	Settlement tephra, Veidivötn component
48.66	1.79	13.61	13.02	0.25	6.46	11.32	2.17	0.26	97.59	Settlement tephra, Veidivötn component
48.52	1.75	13.89	13.14	0.22	6.66	11.63	2.17	0.27	98.29	Settlement tephra, Veidivötn component
48.36	1.94	13.93	12.72	0.20	6.76	11.39	2.37	0.23	97.92	Settlement tephra, Veidivötn component
Section 3A	*0.87 m*		*Potential tephra layer*							
49.25	1.40	13.82	12.84	0.18	6.57	10.88	2.04	0.16	97.18	Veidivötn volcanic system?
48.51	1.88	14.09	12.15	0.17	7.37	12.53	2.11	0.22	99.07	Veidivötn volcanic system?
47.91	1.78	14.92	12.23	0.23	7.00	11.02	2.19	0.21	97.52	Veidivötn volcanic system?
49.83	1.41	15.89	8.74	0.14	7.19	13.69	2.27	0.39	99.60	Glass grain of local origin
48.69	1.83	14.87	10.81	0.16	6.38	11.17	2.64	1.01	97.58	Glass grain of local origin
48.04	1.13	15.59	9.64	0.16	8.09	13.57	1.96	0.29	98.51	Glass grain of local origin
Section 3A	*0.91 m*		*Potential tephra layer, AD 400–500?*							
54.78	3.99	11.47	13.02	0.25	2.05	9.45	2.79	1.04	98.88	Hekla volcanic system?

Table 3 Magnetic and Pb measurements in section 3A used to determine chronology for the past 200 years. Dry bulk density data are also included

Depth (cm)	Dry bulk density (g/cm)	Declination (degrees)	Pb (mg/kg)	Li (mg/kg)	Pb/Li	$^{206}Pb/^{207}Pb$	$^{208}Pb/^{206}Pb$	AD year	±
1	0.55		1.644	16.699	0.098	1.1778	2.0824	1998	1
2	0.69	−44.6	2.028	16.741	0.121	1.1763	2.0817	1993	1
3	0.46		1.480	24.473	0.060	1.1763	2.0810	1989	2
4	0.49	−39.8	1.921	20.907	0.092	1.1727	2.0848	1984	2
5	0.45		2.768	16.131	0.172	1.1687	2.0793	1979	3
6	0.55	−42	2.952	16.173	0.182	1.1701	2.0854	1974	3
7	0.50		3.356	17.048	0.197	1.1705	2.0831	1970	4
8	0.55	−43.5	3.544	18.841	0.188	1.1679	2.0889	1965	4
9	0.55		4.567	19.098	0.239	1.1619	2.0968	1960	5
10	0.55	−39.7	3.684	19.563	0.188	1.1687	2.0895	1955	6
11	0.42		2.751	19.427	0.142	1.1754	2.0824	1950	6
12	0.61	−44.9	2.339	19.829	0.118	1.1784	2.0797	1945	7
13	0.63		2.114	25.851	0.082	1.1788	2.0789	1940	8
14	0.55	−47.6	1.766	22.625	0.078	1.1852	2.0765	1935	9
15	0.51		1.866	25.906	0.072	1.1880	2.0710	1930	9
16	0.73	−49.7	1.204	21.853	0.055	1.1940	2.0701	1925	10
17	0.60		2.049	24.475	0.084	1.1895	2.0809	1920	10
18	0.66	−41.6	1.882	22.244	0.085	1.1879	2.0734	1916	11
19	0.61		1.863	25.558	0.073	1.1891	2.0707	1911	11
20	0.60	−48	1.610	24.276	0.066	1.1932	2.0672	1907	12
21	0.71		1.691	22.461	0.075	1.1940	2.0669	1902	12
22	0.56	−45.9	1.507	25.412	0.059	1.1992	2.0620	1898	13
23	0.68		1.492	29.879	0.050	1.1997	2.0597	1893	13
24	0.51	−48.7	1.511	29.352	0.051	1.1971	2.0645	1888	13
25	0.49		1.306	32.664	0.040	1.2025	2.0573	1884	14
26	0.48	−44.8	1.308	34.890	0.037	1.2007	2.0587	1879	14
27	0.70		1.467	28.071	0.052	1.2003	2.0597	1875	15
28	0.79	−48.2	1.424	53.795	0.026			1870	15
29	0.69		1.128	35.047	0.032	1.1947	2.0665	1866	16
30	0.77	−52.3	1.280	33.837	0.038	1.1967	2.0628	1861	16
31			1.815	34.047	0.053	1.2005	2.0549	1857	17
32	0.70	−48.2	1.656	32.617	0.051	1.2070	2.0503	1852	17
33			1.120	34.909	0.032	1.2018	2.0574	1847	17
34	0.85	−48.7	1.313	31.470	0.042	1.2104	2.0478	1843	18
35			1.225	32.999	0.037	1.2040	2.0564	1838	18
36	0.78	−53	1.189	22.027	0.054	1.2051	2.0555	1834	19
37			1.298	23.438	0.055	1.2077	2.0501	1829	19
38	0.81	−61.3	1.057	17.780	0.059	1.2070	2.0523	1825	20
39			1.126	51.014	0.022	1.2108	2.0499	1820	20
40	0.77	−86.9	0.951	33.471	0.028	1.2102	2.0455	1792	30
41			0.906	33.370	0.027	1.2017	2.0561	1764	39
42	0.72	−70.8	0.929	35.920	0.026	1.2165	2.0398	1737	49
43			0.852	34.739	0.025	1.2143	2.0441	1709	58
44	0.90	−76.2	0.836	30.977	0.027	1.2098	2.0518	1681	68
45			1.023	28.611	0.036	1.2132	2.0461	1653	78
46	0.76	−49.7	1.156	32.543	0.036	1.2058	2.0527	1626	87
47			0.930	33.090	0.028	1.2061	2.0475	1598	97
48	0.72	−76.8	0.957	32.588	0.029	1.2145	2.0458	1570	106
49			1.049	33.509	0.031	1.2053	2.0551	1542	116
50	0.71	−55.7	1.013	35.997	0.028	1.2095	2.0494	1514	126
51			1.093	35.617	0.031	1.2051	2.0550	1487	135
52	0.60	12.8	1.132	44.936	0.025	1.2057	2.0525	1460	129
53			1.053	31.496	0.033	1.2069	2.0552	1435	123
54	0.57	46.5	0.948	27.230	0.035	1.2093	2.0499	1411	118
55			0.861	23.427	0.037	1.2098	2.0494	1389	114

Analytical errors for Pb and Li are 2.2 and 3.5%, respectively (based on 21 replicate measurements of standards). Expanded uncertainties for $^{206}Pb/^{207}Pb$ and $^{208}Pb/^{206}Pb$ are 0.0007 and 0.0014, respectively.

tying together the AMS^{14}C/tephra age model with the age model for the top of the section.

Surface distribution of foraminifera

We collected 41 samples along two surface transects to investigate the relationship between the modern marsh foraminifera and tide levels (Figures 1 and 6). Samples that were barren or contained fewer than 50 foraminifera were removed from the data set, leaving a training set of 22 samples.

The main species that we encountered are the agglutinated species *Jadammina macrescens*, *Paratrochammina* (Lepidoparatrochammina) *haynesi* and *Trochammina ochracea* and the

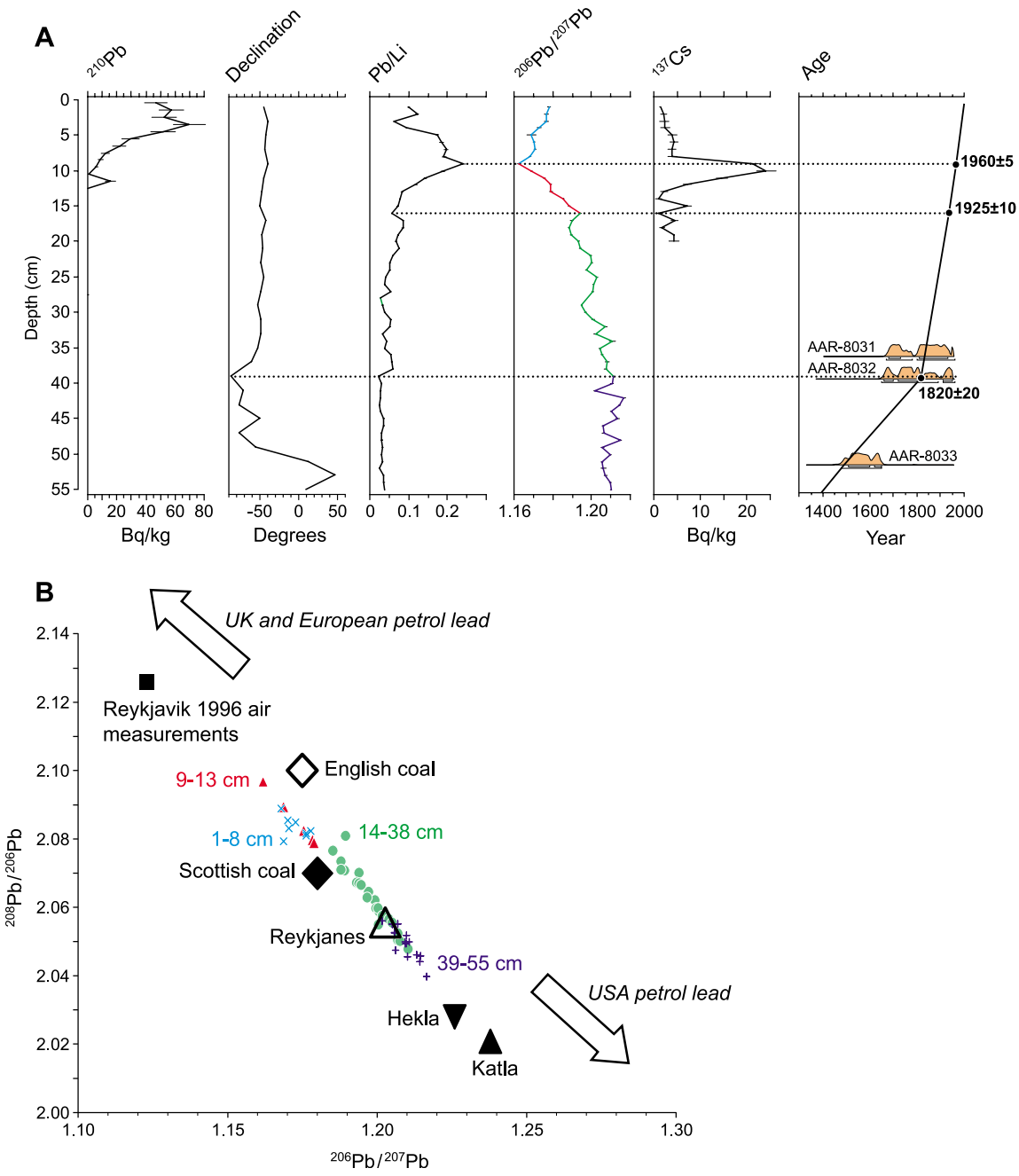

Figure 5 (A) Data to support age model for the top 55 cm of section 3A. Age markers are based on ^{137}Cs, magnetic declination, Pb/Li and ^{206}Pb/^{207}Pb. Pb concentrations are normalized and presented as Pb/Li ratios to account for changes in grain size (Loring, 1991). The ^{210}Pb data are not compatible with other markers and were excluded from the age model. See text for discussion. The 2-σ calibrated probability distributions of the three youngest ^{14}C ages are also shown. (B) Plot of ^{208}Pb/^{206}Pb versus ^{206}Pb/^{207}Pb for Viðarhólmi salt-marsh samples. Four groups of samples are recognized that help to constrain the age model in (A). These groups are: + 39–55 cm (older than ~1820), ○ 14–38 cm (~1820–1925), Δ 9–13 cm (~1925–1960) and × 1–8 cm (~1960–2003). Also plotted are Pb isotopic ratios for Reykjavik 1996 air (Bollhöfer and Rosman, 2001), English and Scottish coal (Shotyk *et al.*, 2005), and three Icelandic volcanic systems (Thirlwall *et al.*, 2004). Petrol data are from Bollhöfer and Rosman (2001). Ratios of UK and European petrol are 1.070–1.097 (^{206}Pb/^{207}Pb) and 2.162–2.180 (^{208}Pb/^{206}Pb). Ratios for USA petrol lead are 1.281–1.396 (^{206}Pb/^{207}Pb) and 1.875–1.951 (^{208}Pb/^{206}Pb)

calcareous species *Haynesina germanica*, *Elphidium williamsoni* and *Cibicides lobatulus*. In transect 1 both agglutinated and calcareous foraminifera were present, while in transect 2 only agglutinated species occurred. The upper limit of foraminifera in the marsh is at 2.12 m above MSL in transect 1 and at 1.94 m above MSL in transect 2. When choosing a suitable regression model to apply to section 3A, using the C^2 program (Juggins, 2003), we found that Weighted Average Partial Least Squares (WA-PLS) regression produced a low Random Mean Standard Error of Prediction (RMSEP) of 0.14 m, but could not accurately reproduce the surveyed height of the fossil section (0.20 m discrepancy). We selected therefore a Weighted Averaging with Tolerance Downweighting (WA-Tol) regression model that produces accurate results, but is less precise than WA-PLS (RMSEP = 0.20 m; Figure 6C). The low precision is due to spatial variability in the vertical distribution of foraminifera across the marsh. For example, in transect 2 agglutinated foraminifera in samples 35–41 are found at lower heights than in transect 1. WA-Tol regression shows that *Jadammina macrescens*, the most abundant species in the core,

Table 4 ^{210}Pb, ^{226}Ra and ^{137}Cs measurements in section 3A

Depth (cm)	Cumulative bulk density (g/cm^3)	^{210}Pb (Bq/kg)	±	^{226}Ra (Bq/kg)	±	Excess ^{210}Pb (Bq/kg)	±	^{137}Cs (Bq/kg)	±	Sed. rate (g/cm^3)	Sed. rate (cm/yr)	^{137}Cs chronology	±
0	0.00												
0.5	0.28	72.45	9.98	27.02	2.63	46.91	7.92	1.51	0.14	0.12	0.21	2000	1
1.5	0.90	76.81	7.95	21.45	2.19	57.18	8.32	2.17	0.61	0.12	0.20	1995	2
2.5	1.47	77.49	9.99	26.86	2.85	52.30	8.73	2.34	1.02	0.12	0.23	1990	3
3.5	1.95	95.26	11.89	27.90	2.67	69.59	10.94	2.49	0.98	0.12	0.26	1986	4
4.5	2.42	80.53	10.70	30.72	2.93	51.47	8.42	4.06	0.98	0.12	0.25	1982	4
5.5	2.92	54.35	9.46	25.95	2.57	29.35	5.88	4.43	0.97	0.12	0.24	1978	5
6.5	3.44	45.61	7.98	24.64	2.39	21.67	4.33	3.98	0.98	0.12	0.23	1974	6
7.5	3.97	36.45	7.16	24.96	2.70	11.87	2.66	4.09	1.06	0.12	0.23	1970	6
8.5	4.52	31.19	5.95	22.68	2.25	8.79	1.89	21.23	1.26	0.12	0.22	1965	7
9.5	5.07	30.83	4.18	25.15	3.57	5.87	1.15	24.18	2.08	0.12	0.24	1961	8
10.5	5.56	26.21	7.87	25.36	2.64	0.88	0.28	14.67	1.28	0.12	0.24	1957	9
11.5	6.07	33.62	6.44	18.48	2.09	15.65	3.48	7.32	0.85	0.12	0.22	1953	9
12.5	6.69	21.80	4.21	22.68	3.49			2.29	0.82				
13.5	7.28												
14.5	7.81												
15.5	8.44			24.02	2.32			1.07	0.70				
16.5	9.10	8.36	5.59	20.99	4.17			7.37	0.89				
17.5	9.73												
18.5	10.37												
19.5	10.97	7.67	3.63	19.98	1.97			1.22	0.81				
20.5	11.63	11.72	4.55	24.03	3.34								
21.5	12.26												
22.5	12.88	8.41	4.13	19.46	3.27			4.60	0.81				
23.5	13.47												
24.5	13.97			32.03	3.46								
25.5	14.46												
26.5	15.05			19.30	2.92			1.86	0.60				
27.5	15.79	5.27	4.34	21.28	2.16			4.33	0.12				
28.5	16.53			20.87	4.39			4.47	1.16				

has an optimum presence on the marsh surface at 1.78 ± 0.19 m above MSL. *Paratrochammina* (Lepidoparatrochammina) *haynesi* is found slightly higher at 1.96 ± 0.24 m above MSL.

Sea-level reconstruction

Each foraminiferal sample is plotted as a sea-level index point (Figure 7) using:

$$S = H - I \quad (1)$$

where S is palaeo-MSL, H is sample height relative to MSL and I is the indicative meaning (ie, palaeomarsh surface height, Figure 6; cf. Gehrels, 1999). The age of each sample is determined from our age models (Figures 4 and 5), while the indicative meaning is computed using a WA-Tol transfer function (Figure 3). The foraminiferal assemblages are similar throughout the record. As a result, the transfer function predicts that the marsh surface at the sample site has remained at a constant height relative to MSL, indicating that the marsh surface has built up largely in tandem with sea-level rise. In Figure 7 the palaeosea-level heights are plotted as black dots. Between AD 1300 and 1500 we do not have sea-level information because of the low counts or absence of foraminifera in our samples.

From the three basal samples (Figure 2B) and the height of the Mediaeval (pumice) Layer on top of the bedrock (Figure 2B) we can plot four additional sea-level index points that represent four positions of mean sea level that have not been affected by compaction. A straight regression line through the median values of the radiocarbon data, and fixed at the height of the Mediaeval (pumice) Layer gives a long-term relative sea-level rise of 0.65 m per 1000 years (Figure 7). This trend line also presents an opportunity to evaluate potential problems of sediment compaction of section 3A. The line falls entirely within the error bands of the MSL reconstruction. Only in the bottom section, where some sand layers occur (Figure 3) and sea-level index points plot below the trend line, do we find evidence of possible vertical displacement by compaction (Figure 7). We therefore accept only the sea-level reconstruction for the past ~1900 years. Bulk density measurements (Figure 3, Table 3) show that the apparent increase in sedimentation rate above 39 cm in the section is not simply an artefact of compaction (cf. Bird *et al.*, 2004). Although there appears to be a trend towards lower bulk densities near the top, relative low bulk densities are also found below 45 cm.

Discussion

Relative sea level in this part of Iceland has risen by about 1.3 m since AD 100 (Figure 7). By comparing the long-term relative sea-level trend (0.65 m per 1000 years) with our sea-level reconstruction, we can identify the following episodes:

(1) sea-level rise exceeding the long-term trend between AD 100 and 500;
(2) sea-level falling relative to the long-term trend between AD 500 and the first half of the nineteenth century;
(3) rapid sea-level rise from AD 1800–1840 until present.

If we assume the absence of a millennial-scale glacio-eustatic component to global sea-level change in the late Holocene (Peltier, 2002), the rate of 0.65 m per 1000 years should

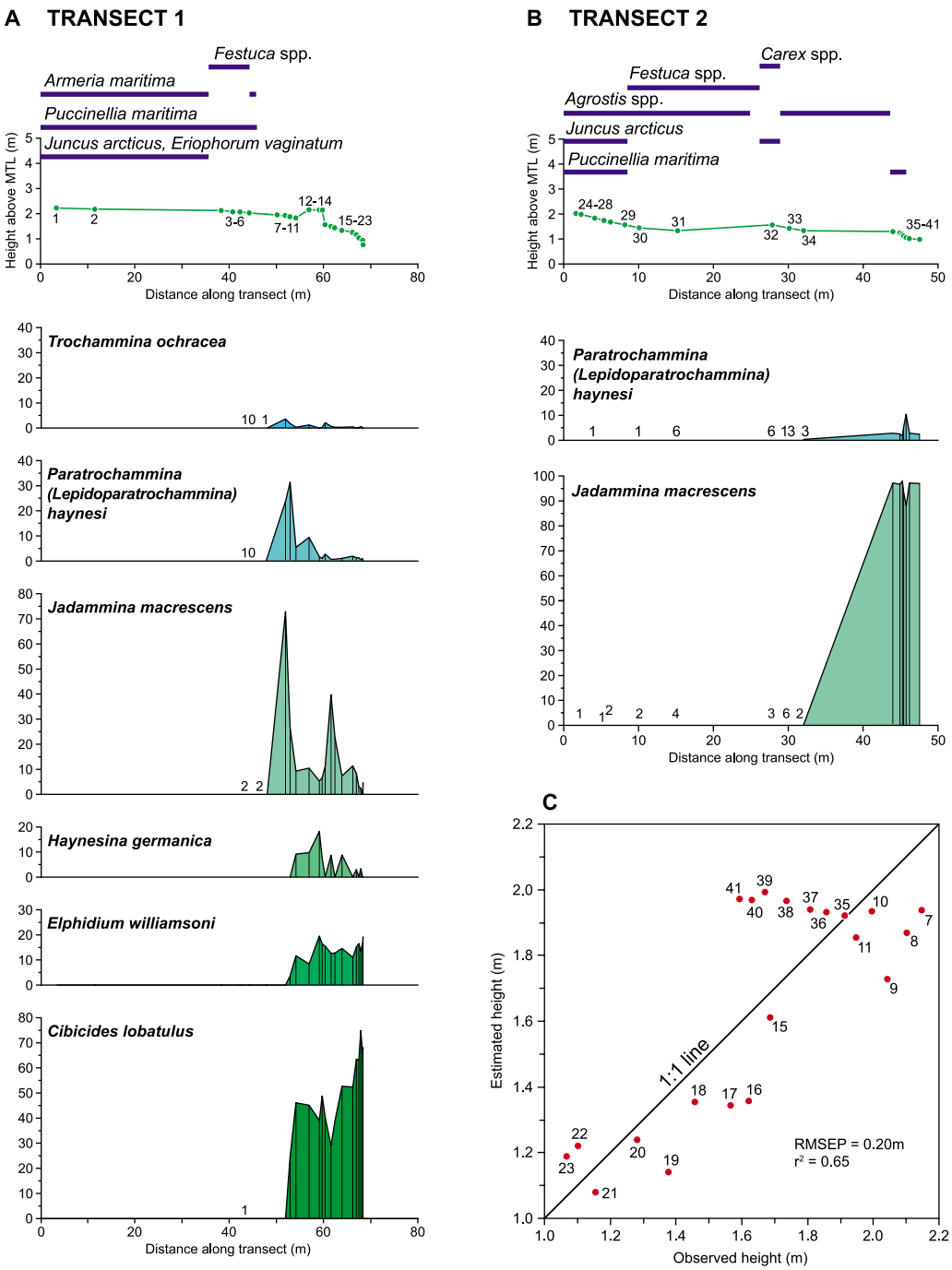

Figure 6 Modern foraminifera in transect 1 (A) and transect 2 (B). Numbers along the horizontal axes are raw counts in samples that contained fewer than 50 specimens. The plot of observed versus predicted heights (C) indicates that foraminifera can be used as a predictive sea-level tool with a precision of ± 0.20 m

approximate the long-term rate of isostatic subsidence for this coastal region of western Iceland. To interpret the centennial-scale changes that are superimposed on the long-term millennial-scale relative sea-level rise, we remove this long-term trend and compare our detrended sea-level record in Figure 8 with the water-temperature reconstruction of Knudsen *et al.* (2004) from core MD992275 collected from the northern Icelandic shelf. The falling (detrended) sea level in western Iceland through most of the past millennium coincides with a cooling of surface and bottom waters of $\sim 1.8^{\circ}$C since AD 800 (Knudsen *et al.*, 2004). This comparison holds on centennial timescales; on subcentennial timescales the water-temperature records shows considerable variability. The correspondence with seawater temperature trends would suggest that steric effects are an important component of relative sea-level changes in the North Atlantic Ocean in the last millennium. To account for the observed sea-level fall would require the suggested cooling of $\sim 1.8^{\circ}$C to occur over a typical mean mixed ocean layer of 400 m, a depth broadly consistent with present-day hydrographic data (Marine Research Institute, 2006).

It is well known that sea-level rise during the past century contains an important steric component (Church *et al.*, 2001). Recent studies have shown that steric effects are regionally highly variable, but overall they contribute significantly to the global sea-level signal observed by satellites in the past decade (Cazenave and Nerem, 2004). It is therefore not unreasonable

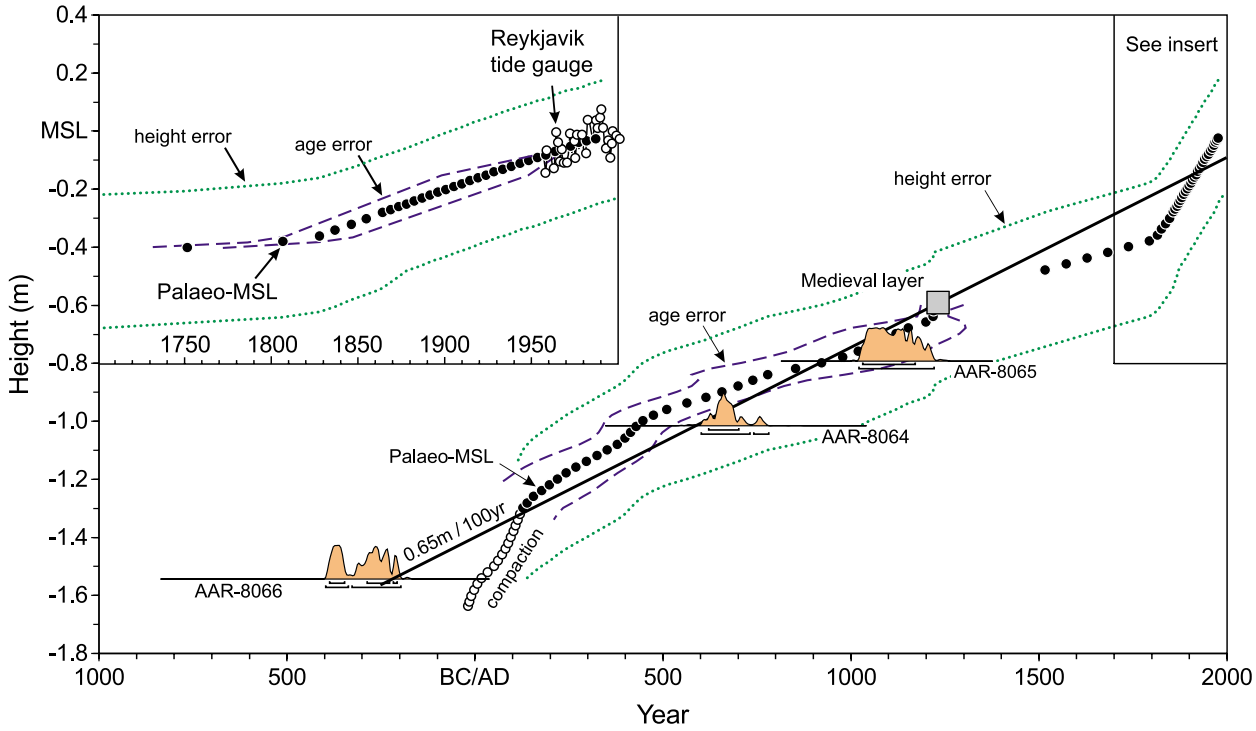

Figure 7 Relative sea-level changes at Viðarhólmi. Solid circles represent reconstructed sea-level positions. The trend line through the Mediaeval Pumice sea-level index point and the three basal peat index points (Figure 2B) shows a long-term sea-level rise of 0.65 m per 1000 years. The position of oldest samples below the trend line may indicate some compaction in the lower part of the core where sand layers occur (Figure 3). The youngest part of the reconstruction corresponds well with sea-level observations at Reykjavik (PSMSL 2004). The recent acceleration of sea-level rise is dated to 1800–1840

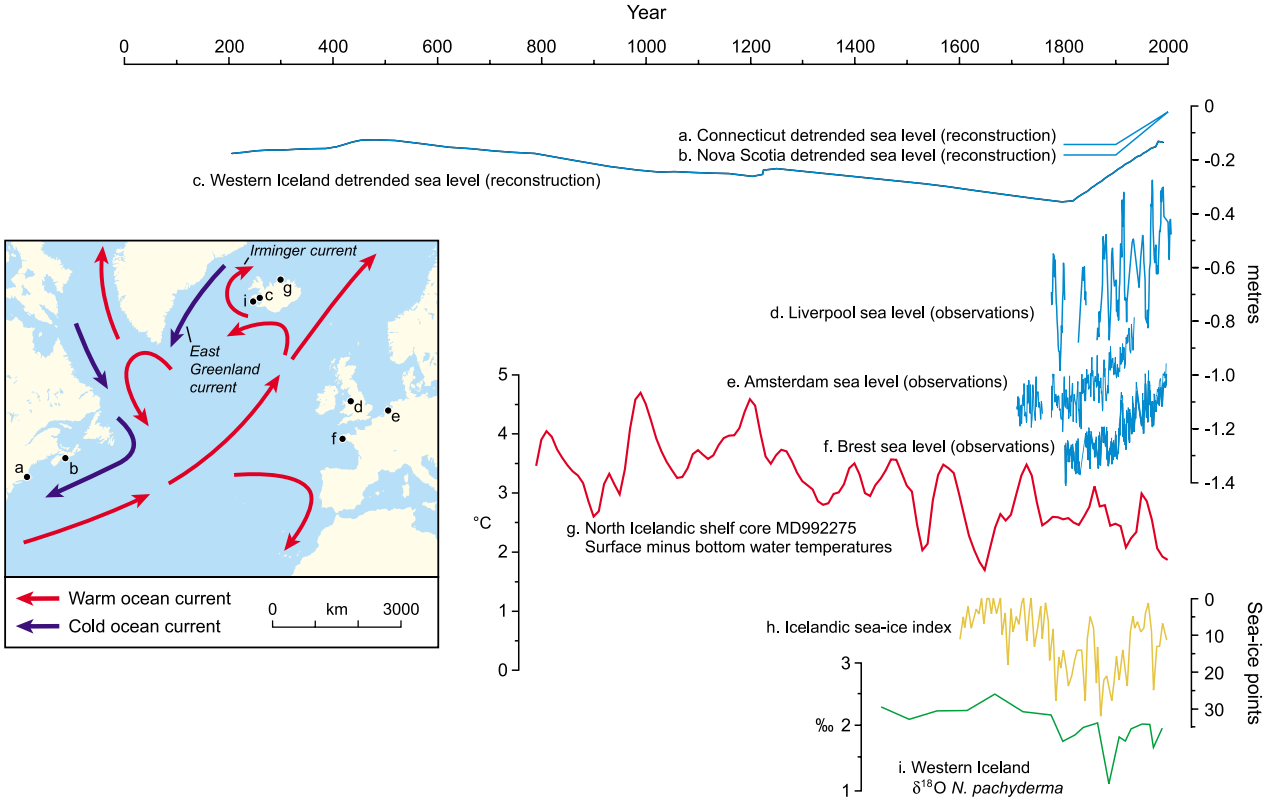

Figure 8 Comparison of western Iceland sea-level record with other sea-level records and climatic proxies. The Iceland sea-level record (c) is detrended by subtracting a rate of 0.65 m per 1000 years, which is attributable to isostatic subsidence (see text). Sources: a, Donnelly *et al.* (2004); b, Gehrels *et al.* (2005); d, PSMSL (2004) and Woodworth (1999); e–f, PSMSL (2004); g, Knudsen *et al.* (2004); h, Ogilvie and Jónsdottir (1996), cited in Jennings *et al.* (2001); i, Jennings *et al.* (2001). The sea-ice index (h) is based on a point system in which a year is awarded a sea-ice point if one of four regions of Iceland reported the presence of sea ice in a season. For example, a year in which sea ice was reported off the northern coasts in spring and summer, and the eastern coasts in spring only, would be allotted a total of three sea-ice points (Ogilvie, 1996)

to suspect that steric changes have left an imprint in the sea-level signal of western Iceland on centennial timescales in the past millennium. A further test of this hypothesis would be provided if the water-temperature record is extended back to before AD 500, when a change from a positive to a negative sea-level trend occurred (Figure 8).

The most remarkable feature of the recent sea-level record is the sharp rise of about 0.4 m since 1800–1840. The rise is manifested by a sudden increase in the sedimentation rate of the salt marsh. For the purpose of this study it is important to note that despite this change in sedimentation rate the foraminiferal assemblages in the section remained unchanged (Figure 3), indicating that the higher rates of sedimentation since the first half of the nineteenth century are a response to an increase in the rate of sea-level rise and that the marsh has been able to keep pace with sea-level rise. The rapid sea-level rise is not reflected in the records of seawater temperatures (Figure 8; Knudsen *et al.*, 2004), which remained relatively cool. The Icelandic sea-ice index shows severe sea-ice conditions that persisted around Iceland between 1780 and 1920 (Figure 8; Ogilvie and Jónsdottir, 1996, cited in Jennings *et al.*, 2001). Low oxygen-isotope ratios of the planktonic foraminifer *Neogloboquadrina pachyderma* in a core from Faxafloi Bay are interpreted as reduced salinities resulting from sea-ice invasions during this time (Figure 8; Jennings *et al.*, 2001). Warming of surface waters around Iceland only occurred after ~1920, so that the rapid sea-level rise that started in the middle of the nineteenth century is best explained as a far-field glacio-eustatic signal.

The last 50 years of our reconstruction correspond well with the rate of sea-level rise of 2.3 ± 0.5 mm/yr measured at Reykjavik since 1957 (Woodworth and Player, 2003; PSMSL, 2004; Figure 7). This agreement with observational sea-level data supports the robustness of the sea-level reconstruction (Gehrels *et al.*, 2005).

In Figure 8 we show five sea-level records for the past two centuries. Two are recent reconstructions from northeastern North America (Connecticut and Nova Scotia), whereas the other three are some of the longest European sea-level observations (Liverpool, Amsterdam, Brest). In northeastern North America, the onset of rapid recent sea-level rise occurred between 1880 and 1920 (Donnelly *et al.*, 2004; Gehrels *et al.*, 2005), about half a century later than in Iceland (Figure 8). Similar to Iceland, the longest instrumental sea-level records from Europe show that sea-level rise accelerated during the middle of the nineteenth century.

Model simulations indicate that the heat content of the oceans started to increase in the mid-nineteenth century (Crowley *et al.*, 2003), but instrumental measurements show that steric changes are spatially highly non-uniform (Cazenave and Nerem, 2004). The difference in timing of the onset of recent rapid sea-level rise between the (north)eastern and the western Atlantic Ocean may therefore be due to the different characteristics of the water masses and the influence of the North Atlantic Oscillation (NAO). For example, positive steric trends in the Gulf Stream region and negative trends in the subpolar gyre for the period 1950–1990 resemble an NAO pattern (Cazenave and Nerem, 2004). Furthermore, along the coasts of Newfoundland and Nova Scotia, salinity is a factor in controlling steric sea level on multidecadal to centennial timescales, while further south, along the US East Coast, sea level is also influenced by the position of the Gulf Stream (van der Schrier *et al.*, 2004). High-resolution sea surface and sea bottom temperature and salinity records from the western Atlantic (and elsewhere) can shed further light on the hypothesis that steric changes have played an important role in North Atlantic sea-level variability, not only on decadal timescales, but also on multidecadal to centennial timescales.

Conclusions

(1) Relative sea level on the west coast of Iceland has risen by 1.3 m since AD 100 and contains a long-term isostatic subsidence component of ~0.65 m per 1000 years. During the past 1200 years, estimated steric effects produced by cooling of surface and bottom waters off Iceland are broadly consistent with the sea-level record after the latter has been detrended for long-term isostatic subsidence.

(2) Sea level off western Iceland began to rise abruptly between 1800 and 1840 as dated by palaeomagnetism, Pb concentrations and Pb isotopes. The change carries the signature of industrial activities as it occurred around the time of a rise in Pb fallout produced by European coal burning. Until ~1920 ocean waters remained relatively cold and steric change cannot explain the rise. It is therefore thought to be primarily produced by far-field melting of land ice in response to global temperature rise. Differences in the timing of the onset of rapid sea-level rise across the North Atlantic Ocean may reflect spatial non-uniformity of steric sea-level change on multidecadal to centennial timescales.

(3) The last 50 years of our reconstruction matches the trend measured by the Reykjavik tide gauge since 1957 of 2.3 ± 0.5 mm/yr. Precise and well-dated sea-level proxy records from salt-marsh deposits offer useful supplements to the small data base of long-tide gauge records. They are of great value for documenting the spatial and temporal patterns of sea-level rise in the past 200 years and, ultimately, for determining the causes of this rise.

Acknowledgements

This research was undertaken as part of HOLSMEER (Late Holocene Shallow Marine Environments of Europe), a European project funded under the 'Energy, Environment and Sustainable Development' programme of the Fifth Framework (contract EVK2-CT-2000-00060). Simon Newman (Plymouth) identified the foraminifera. Andreas Prokoph (SPEEDSTAT, Ottawa) performed statistical radiocarbon age-modelling analyses. Andrew Roberts (Southampton) provided magnetic data. Andrew Fisher (Plymouth) measured Pb and Li concentrations. Robert Clough and Hywel Evans (Plymouth) assisted with Pb isotope analyses. Margaret Grimbly (Plymouth) prepared tephra slides for microprobe analyses. Ole Tumyr (Bergen) provided help with microprobe analyses. Sigurdur Steinthorsson (University of Iceland) supplied background data on Snæfellsnes volcanics. Leifur Simonarson (University of Iceland) identified the horse bone described in section 2A. Peter Appleby (Liverpool) helped with the interpretation of the ^{210}Pb and ^{137}Cs results. Jamie Quinn (Plymouth) assisted with the drawing of figures. We thank Bryndis Robertsdottir (University of Iceland) and University of Plymouth students Dylan FitzPatrick and Adam Smith for help in the field and Andy Plater (Liverpool) and Philip Woodworth (Proudman Oceanographic Laboratory) for their constructive reviews. This paper is a contribution to IGCP-Project 495 ('Late Quaternary Land–Ocean Interactions: Driving Mechanisms and Coastal Responses').

Appendix

Major element geochemical analyses of volcanic glass shards of non-determinable sources in sections 1 and 3A. Note that P_2O_5 was analysed in section 1, but not in section 3A. MnO was analysed in section 3A, but not in section 1.

SiO_2	TiO_2	Al_2O_3	FeO	MgO	CaO	Na_2O	K_2O	P_2O_5	Sum	Origin
Section 1	0.35 m									
69.99	0.31	13.38	3.94	0.21	1.33	4.98	3.42	0.22	97.76	Glass grain of local origin
66.65	0.49	16.13	4.68	0.33	1.99	5.08	4.11	0.07	99.53	Glass grain of local origin
62.51	1.46	15.87	6.24	1.27	3.03	4.78	4.41	0.35	99.91	Glass grain of local origin
48.89	3.76	14.57	12.34	3.89	8.55	3.68	1.92	0.83	98.43	Glass grain of local origin
48.53	1.87	15.80	11.07	7.05	11.82	2.76	0.50	0.38	99.79	Glass grain of local origin
48.41	1.49	15.93	9.63	8.25	13.25	1.91	0.67	0.26	99.80	Glass grain of local origin
Section 1	0.55 m									
64.92	1.23	13.91	5.92	1.24	3.10	4.81	2.72	0.19	98.04	Katla volcanic system
50.48	3.09	15.36	11.11	3.99	7.97	3.97	1.98	0.88	98.82	Glass grain of local origin
49.57	1.85	13.72	13.46	6.42	11.24	2.39	0.18	0.14	98.98	Glass grain of local origin
49.42	1.67	15.76	9.91	7.06	11.89	2.28	0.88	0.29	99.15	Glass grain of local origin
64.92	1.23	13.91	5.92	1.24	3.10	4.81	2.72	0.19	98.04	Katla volcanic system
Section 1	1.25 m									
68.07	0.31	15.49	3.65	0.10	1.35	4.92	4.63	0.00	98.51	Glass grain of local origin
67.87	0.18	14.97	3.00	0.14	1.07	5.01	4.85	0.05	97.15	Glass grain of local origin
64.11	0.97	15.37	7.23	1.15	4.37	4.51	1.66	0.26	99.63	Hekla volcanic system
63.00	1.00	15.70	7.22	1.27	4.39	3.94	1.61	0.45	98.57	Hekla volcanic system
47.50	3.02	15.87	11.36	4.28	8.33	3.90	1.90	1.25	97.41	Glass grain of local origin
49.68	2.09	14.85	11.32	5.23	10.50	2.77	1.40	0.41	98.25	Glass grain of local origin
50.43	1.96	15.65	10.91	5.02	10.63	2.87	1.30	0.49	99.27	Glass grain of local origin
49.13	1.81	15.66	10.42	6.47	11.16	2.39	1.04	0.22	98.32	Glass grain of local origin
49.01	1.80	13.60	13.93	6.36	10.49	2.38	0.20	0.26	98.03	Veidivötn volcanic system?
68.07	0.31	15.49	3.65	0.10	1.35	4.92	4.63	0.00	98.51	Glass grain of local origin
Section 1	1.35 m									
47.61	4.63	11.74	16.58	4.63	9.00	2.41	0.67	0.37	97.63	Glass grain of local origin
49.22	1.76	15.68	10.83	6.54	11.83	2.38	1.01	0.33	99.57	Glass grain of local origin
48.06	1.39	15.91	10.09	9.03	12.53	1.76	0.47	0.18	99.41	Glass grain of local origin
50.65	1.18	15.36	9.81	7.74	11.00	1.97	0.47	0.04	98.20	Glass grain of local origin
Section 3A	0.09 m									
64.66	0.90	16.28	4.99	0.19	0.64	2.98	4.64	4.51	99.84	Glass grain of local origin
60.78	1.63	15.68	7.01	0.19	1.97	4.24	5.11	2.97	99.62	Glass grain of local origin
60.37	1.57	15.39	8.04	0.27	1.97	4.27	4.42	2.20	98.53	Glass grain of local origin
58.03	1.42	16.06	7.09	0.23	1.84	4.45	4.68	3.34	97.19	Glass grain of local origin
49.64	1.87	14.95	10.16	0.19	6.27	11.75	1.95	0.98	97.79	Glass grain of local origin
49.18	1.63	14.82	10.44	0.20	6.89	12.04	2.37	0.66	98.28	Glass grain of local origin
49.18	1.55	15.18	10.14	0.20	6.72	11.98	2.29	0.94	98.22	Glass grain of local origin
48.84	1.92	15.98	10.61	0.16	6.64	10.74	2.51	1.10	98.55	Glass grain of local origin
48.58	1.66	15.69	9.90	0.16	7.04	11.79	2.35	0.96	98.18	Glass grain of local origin
48.07	2.16	15.76	11.18	0.23	6.89	11.16	2.59	0.99	99.07	Glass grain of local origin
47.90	2.00	15.81	11.12	0.21	6.76	10.86	2.45	1.00	98.15	Glass grain of local origin
50.24	1.89	13.69	13.49	0.23	6.78	11.08	2.46	0.22	100.12	Volc. syst. outside Snæfellsnes
48.47	1.85	14.08	11.97	0.15	7.39	12.36	2.01	0.24	98.57	Volc. syst. outside Snæfellsnes
Section 3A	0.14 m									
63.50	0.97	16.43	5.88	0.29	0.91	3.56	4.71	3.37	99.66	Glass grain of local origin
59.04	1.49	16.17	7.19	0.15	1.65	4.01	4.62	3.13	97.49	Glass grain of local origin
49.52	1.77	13.65	13.15	0.24	6.70	10.73	1.95	0.21	97.95	Volc. syst. outside Snæfellsnes
49.23	1.72	15.72	10.15	0.21	6.72	11.47	2.25	0.99	98.48	Glass grain of local origin
48.71	2.00	15.55	10.99	0.13	7.26	11.27	2.52	1.06	99.52	Glass grain of local origin
48.06	1.82	15.50	10.35	0.20	7.56	12.25	2.30	0.54	98.62	Glass grain of local origin
48.04	1.49	15.40	8.94	0.18	9.22	13.26	1.87	0.66	99.11	Glass grain of local origin
47.58	2.25	14.30	12.14	0.25	6.06	11.63	2.43	1.11	97.80	Glass grain of local origin
Section 3A	0.175 m									
63.71	0.66	16.20	5.17	0.25	0.53	2.46	5.06	3.83	97.89	Glass grain of local origin
51.01	2.99	14.94	10.80	0.31	3.97	7.89	3.76	1.90	97.61	Glass grain of local origin
47.26	2.86	13.75	12.68	0.29	6.35	12.12	3.79	0.94	100.07	Glass grain of local origin
47.94	1.77	15.87	10.28	0.18	7.34	11.77	2.42	0.50	98.10	Glass grain of local origin
47.86	1.51	15.70	9.12	0.16	8.44	12.93	1.95	0.60	98.31	Glass grain of local origin
48.12	1.40	15.55	9.24	0.18	8.99	13.40	1.90	0.54	99.37	Glass grain of local origin

Appendix (*continued*)

SiO_2	TiO_2	Al_2O_3	FeO	MgO	CaO	Na_2O	K_2O	P_2O_5	Sum	Origin
47.82	1.40	15.47	9.07	0.17	8.49	13.62	1.83	0.51	98.42	Glass grain of local origin
47.86	1.37	15.38	9.35	0.11	8.81	13.29	1.82	0.58	98.60	Glass grain of local origin
47.43	1.37	15.32	9.03	0.12	8.98	12.89	1.69	0.58	97.45	Glass grain of local origin
47.40	1.12	15.95	9.23	0.17	8.52	13.03	2.08	0.22	97.77	Glass grain of local origin
70.20	0.26	14.68	2.19	0.02	0.21	0.84	4.49	4.59	97.53	Volc. syst. outside Snæfellsnes
49.62	2.24	13.47	13.30	0.26	6.33	10.37	2.62	0.33	98.56	Volc. syst. outside Snæfellsnes
49.86	1.58	13.87	12.32	0.21	7.37	11.52	1.95	0.14	98.86	Volc. syst. outside Snæfellsnes
48.57	1.54	14.48	11.57	0.21	7.53	12.28	2.03	0.24	98.48	Volc. syst. outside Snæfellsnes
Section 3A	0.21 m									
49.23	1.80	14.90	10.54	0.25	6.74	11.68	2.33	0.97	98.48	Glass grain of local origin
48.99	1.52	15.82	10.14	0.26	7.99	12.40	2.08	0.48	99.71	Glass grain of local origin
48.34	1.67	15.55	10.52	0.23	7.67	12.33	2.32	0.49	99.15	Glass grain of local origin
46.93	3.16	13.54	12.35	0.22	6.10	11.72	2.53	0.85	97.44	Glass grain of local origin
46.61	3.11	12.84	12.52	0.25	6.52	11.90	2.80	0.93	97.50	Glass grain of local origin
46.27	3.13	13.46	12.55	0.15	6.43	11.81	2.66	0.92	97.41	Glass grain of local origin
49.81	1.85	13.18	12.13	0.16	6.81	11.47	2.51	0.27	98.22	Volc. syst. outside Snæfellsnes
Section 3A	0.305 m									
54.21	1.65	12.22	11.43	0.15	5.67	10.53	1.96	0.21	98.07	Glass grain of local origin?
49.67	1.76	15.17	10.40	0.19	5.67	10.63	2.10	1.06	96.69	Glass grain of local origin
48.81	1.80	15.40	10.24	0.18	6.49	10.25	2.38	1.11	96.69	Glass grain of local origin

References

Admiralty Tide Tables 2001: *Volume 2, Europe (excluding United Kingdom and Ireland)*. UK Hydrographic Office.

Allen, J.R.L. 1990: Constraints on measurement of sea-level movements from saltmarsh accretion rates. *Journal of the Geological Society* 147, 5–7.

Andrews, J.T. and **Giraudeau, J.** 2003: Multi-proxy records showing significant Holocene environmental variability: the inner N. Iceland shelf (Hunafloi). *Quaternary Science Reviews* 22, 175–93.

Andrews, J.T., Hardadottir, J., Stoner, J.S., Mann, M.E., Kristjansdottir, G.B. and **Koc, N.** 2003: Decadal to millennial-scale periodicities in North Iceland shelf sediments over the last 12000 cal yr: long-term North Atlantic oceanographic variability and solar forcing. *Earth and Planetary Science Letters* 210, 453–65.

Angelier, J., Slunga, R., Bergerat, F., Stefansson, R. and **Homberg, C.** 2004: Perturbation of stress and oceanic rift extension across transform faults shown by earthquake focal mechanisms in Iceland. *Earth and Planetary Science Letters* 219, 271–84.

Barraclough, D.R., Carrigan, J.G. and **Malin, S.R.C.** 2000: Observed geomagnetic field intensity in London since 1820. *Geophysical Journal International* 141, 83–99.

Bindler, R., Renberg, I., Anderson, N.J., Appleby, P.G., Emteryd, O. and **Boyle, J.** 2001: Pb isotope ratios of lake sediments in West Greenland: inferences on pollution sources. *Atmospheric Environment* 35, 4675–85.

Bird, M.I., Fifield, L.K., Chua, S. and **Goh, B.** 2004: Calculating sediment compaction for radiocarbon dating of intertidal sediments. *Radiocarbon* 46, 421–35.

Bollhöfer, A. and **Rosman, K.J.R.** 2001: Isotopic source signatures for atmospheric lead: the Northern Hemisphere. *Geochimica et Cosmochimica Acta* 65, 1727–40.

Candelone, J.-P., Hong, S., Pellone, C. and **Boutron, C.F.** 1995: Post-indistrial revolution changes in large-scale atmospheric pollution of the northern hemisphere by heavy metals as documented in central Greenland snow and ice. *Journal of Geophysical Research* 100, 16 605–16.

Cazenave, A. and **Nerem, R.S.** 2004: Present-day sea level change: observations and causes. *Reviews of Geophysics* 42, RG3001, doi:10.1029/2003RG000139.

Church, J.A. and **White, N.J.** 2006: A 20th century acceleration in global sea-level rise. *Geophysical Research Letters* 33, L01602, doi:10.1029/2005GL024826.

Church, J.A., Gregory, J.M., Huybrechts, P., Kuhn, M., Lambeck, K., Nhuan, M.T., Qin, D. and **Woodworth, P.L.** 2001: Changes in sea level. In Houghton, J.T., Ding, Y., Griggs, D.J., Noguer, M., van der Linden, P.J., Dai, X., Maskell, K. and Johnson, C.A., editors, *Climate change 2001: the scientific basis*. Contribution of Working Group I to the Third Assessment Report of the Intergovernmental Panel on Climate Change. Cambridge University Press, 639–93.

Crowley, T.J., Baum, S.K., Kim, K.-Y., Hegerl, G.C. and **Hyde, W.T.** 2003: Modeling ocean heat content changes during the past millennium. *Geophysical Research Letters* 30, doi:10.1029/2003GL017801.

Donnelly, J.P., Cleary, P., Newby, P. and **Ettinger, R.** 2004: Coupling instrumental and geological records of sea-level change: evidence from southern New England of an increase in the rate of sea-level rise in the late 19th century. *Geophysical Research Letters* 31, doi:10.1029/2003GL018933.

Douglas, B.C. 1992: Global sea level acceleration. *Journal of Geophysical Research* 97, 12 699–706.

Dugmore, A.J. 1989: Icelandic volcanic ash in Sccotland. *Scottish Geographical Magazine* 105, 168–72.

Dugmore, A.J., Newton, A.J., Sugden, D.E. and **Larsen, G.** 1992: Geochemical stability of fine-grained silicic Holocene tephra in Iceland and Scotland. *Journal of Quaternary Science* 7, 173–83.

Eades, L.J., Farmer, J.G., MacKenzie, A.B., Kirika, A. and **Bailey-Watts, A.E.** 2002: Stable lead isotopic characterisation of the historical record of environmental lead contamination in dated freshwater lake sediment cores from northern and central Scotland. *Science of the Total Environment* 292, 55–67.

Farmer, J.G., Eades, L.J. and **Graham, M.C.** 1999: The lead content and isotopic composition of British coals and their implications for past and present releases of lead to the U.K. environment. *Environmental Geochemistry and Health* 21, 257–72.

Gehrels, M.J., Lowe, D.J., Hazell, Z.J. and **Newnham, R.M.** 2006: A continuous 5300-yr Holocene cryptotephrostratigraphic record

from northern New Zealand and implications for tephrochronology and volcanic hazard assessment. *The Holocene* 16, 173–87.
Gehrels, W.R. 1999: Middle and late Holocene sea-level changes in eastern Maine reconstructed from foraminiferal saltmarsh stratigraphy and AMS C-14 ages on basal peat. *Quaternary Research* 52, 350–59.
——— 2000: Using foraminiferal transfer functions to produce high-resolution sea-level records from saltmarsh deposits, Maine, USA. *The Holocene* 10, 367–76.
——— 2002: Intertidal foraminifera as palaeoenvironmental indicators. In Haslett, S.K., editor, *Quaternary environmental micropalaeontology*. Arnold, 91–114.
Gehrels, W.R. and **Newman, S.W.G.** 2004: Salt-marsh foraminifera in Ho Bugt, western Denmark, and their use as sea-level indicators. *Danish Journal of Geography* 104, 49–58.
Gehrels, W.R. and **van de Plassche, O.** 1999: The use of *Jadammina macrescens* (Brady) and *Balticammina pseudomacrescens* Brönnimann, Lutze and Whittaker (Protozoa: Foraminiferida) as sea-level indicators. *Palaeogeography, Palaeoclimatology, Palaeoecology* 149, 89–101.
Gehrels, W.R., Kirby, J.R., Prokoph, A., Newnham, R.M., Achterberg, E.P., Evans, H., Black, S. and **Scott, D.B.** 2005: Onset of recent rapid sea-level rise in the western Atlantic Ocean. *Quaternary Science Reviews* 24, 2083–100
Grönvold, K., Oskarsson, N., Johnsen, S.J., Clausen, H.B., Hammer, C.U., Bond, G. and **Bard, E.** 1995: Ash layers from Iceland in the Greenland GRIP ice core correlated with oceanic and land sediments. *Earth and Planetary Science Letters* 135, 149–55.
Haflidason, H., Larsen, G. and **Olafsson, G.** 1992: The recent sedimentation history of Thingvallavatn, Iceland. *Oikos* 64, 80–95.
Hansom, J.D. and **Briggs, D.J.** 1991: Sea-level change in Vestfirdir, north west Iceland. In Maizels, J.K. and Caseldine, C., editors, *Environmental change in Iceland: past and present*. Kluwer Academic Publishers, 79–91.
Ingólfsson, A. 1994: Species assemblages in saltmarsh ponds in western Iceland in relation to environmental variables. *Estuarine Coastal and Shelf Science* 38, 235–48.
——— 1998: Sjávarfitjar. In Ólafsson, J.S. editor, *Íslensk votlendi-verndun og nýting*. Háskólaútgáfan, 57–68.
Ingólfsson, O. and **Norddahl, H.** 2001: High relative sea level during the Bolling Interstadial in western Iceland: a reflection of ice-sheet collapse and extremely rapid glacial unloading. *Arctic Antarctic and Alpine Research* 33, 231–43.
Ingólfsson, O., Norddahl, H. and **Haflidason, H.** 1995: Rapid isostatic rebound in southwestern Iceland at the end of the last glaciation. *Boreas* 24, 245–59.
Jackson, A., Jonkers, A.R.T. and **Walker, M.R.** 2000: Four centuries of geomagnetic secular variation from historical records. *Philosophical Transactions of the Royal Society of London Series A-Mathematical Physical and Engineering Sciences* 358, 957–90.
Jennings, A.E., Hagen, S., Hardardottir, J., Stein, R., Ogilvie, A.E.J. and **Jónsdottir, I.** 2001: Oceanographic change and terrestrial human impacts in a post AD 1400 sediment record from the southwest Iceland shelf. *Climatic Change* 48, 83–100.
Jóhannesson, H. 1977: Þar var ei bærinn, sem nú er borgin. *Náttúrufrædinguinn* 47, 129–204.
Jonkers, A.R.T., Jackson, A. and **Murray, A.** 2003: Four centuries of geomagnetic data from historical records. *Reviews of Geophysics* 41, doi:10.1029/2002RG000115.
Juggins, S. 2003: *C^2 user guide. Software for ecological and palaeoecological data analysis and visualisation*. University of Newcastle, 69 pp.
Knudsen, K.L., Eiriksson, J., Jansen, E., Jiang, H., Rytter, F. and **Gudmundsdottir, E.R.** 2004: Palaeoceanographic changes off North Iceland through the last 1200 years: foraminifera, stable isotopes, diatoms and ice rafted debris. *Quaternary Science Reviews* 23, 2231–46.
Loring, D.H. 1991: Normalisation of heavy-metal data from estuarine and coastal sediments. *Journal of Marine Science* 48, 101–15.
Malin, S.R.C. and **Bullard, E.** 1981: The direction of the Earth's magnetic field at London, 1570–1975. *Philosophical Transactions of the Royal Society of London Series A-Mathematical Physical and Engineering Sciences* 299, 357–423.
Marine Research Institute 2006: Hafrannsóknastofnunin. Retrieved 17 May 2006 from http://www.hafro.is/Sjora/
Norddahl, H. and **Einarsson, Th.** 2001: Concurrent changes of relative sea-level and glacier extent at the Weichselian–Holocene boundary in Berufjordur, Eastern Iceland. *Quaternary Science Reviews* 20, 1607–22.
Norddahl, H. and **Petursson, H.** 2005: Relative sea-level change in Iceland: new aspects of the Weichselian deglaciation of Iceland. In Caseldine, C., Russell, A., Hardardottir, J. and Knudsen, O., editors, *Iceland – modern processes and past environments*. Elsevier, 25–78.
Ogilvie, A.E.J. 1996: Sea-ice conditions off the coasts of Iceland A.D. 1601–1850 with special reference to part of the Maunder Minimum period (1675–1715). In Pedersen, E.S., editor, *North European climate data in the latter part of the Maunder Minimum period A.D. 1675–1715*. AmS-Varia 25, Museum of Archaeology, Stavanger, 9–12.
Ogilvie, A.E.J. and **Jónsdottir, I.** 1996: Sea-ice indices off the coasts of Iceland: evidence from historical data and early sea-ice maps. *26th International Arctic Workshop, Arctic and Alpine Environments, Past and Present Program with Abstracts*. Institute of Alpine and Arctic Research (INSTAAR), Boulder CO, 14–16 March 1996, 109–10.
Pálsson, S.E., Egilsson, K., Thórisson, S., Magnússon, S.M., Ólafsdóttir, E.D. and **Indridason, K.** 1994: Transfer of radiocaesium from soil and plants to reindeer in Iceland. *Journal of Environmental Radioactivity* 24, 107–25.
Peltier, W.R. 2002: On eustatic sea level history: Last Glacial Maximum to Holocene. *Quaternary Science Reviews* 21, 377–96.
Permanent Service for Mean Sea Level (PSMSL) 2004: Permanent service for Mean Sea Level. Retrieved 17 May 2006 from http://www.pol.ac.uk/psmsl
Preiss, N., Mélières, M.-A. and **Pourchet, M.** 1996: A compilation of data on lead 210 concentration in surface air and fluxes at the air–surface and water–sediment interfaces. *Journal of Geophysical Research* 101, D22, 28847–62.
Reimer, P.J., Baillie, M.G.L., Bard, E., Bayliss, A., Beck, J.W., Bertrand, C., Blackwell, P.G., Buck, C.E., Burr, G., Cutler, K.B., Damon, P.E., Edwards, R.L., Fairbanks, R.G., Friedrich, M., Guilderson, T.P., Hughen, K.A., Kromer, B., McCormac, F.G., Manning, S., Bronk Ramsey, C., Reimer, R.W., Remmele, S., Southon, J.R., Stuiver, M., Talamo, S., Taylor, F.W., van der Plicht, J. and **Weyhenmeyer C.E.** 2004: IntCal04 terrestrial radiocarbon age calibration, 26–0 ka BP. *Radiocarbon* 46, 1029–58.
Rundgren, M., Ingólfsson, O., Bjorck, S., Jiang, H. and **Haflidason, H.** 1997: Dynamic sea-level change during the last deglaciation of northern Iceland. *Boreas* 26, 201–15.
Schwikowski, M., Barbante, C., Doering, T., Gaeggeler, H.W., Boutron, C., Schotterer, U., Tobler, L., van de Velde, K., Ferrari, C., Cozzi, G., Rosman, K. and **Cescon, P.** 2004: Post-17th-century changes of European lead emissions recorded in high-altitude apline snow and ice. *Environmental Science and Technology* 38, 957–64.
Shotyk, W., Goodsite, M.E., Roos-Barraclough, F., Frei, R., Heinemeier, J., Asmund, G., Lohse, C. and **Hansen, T.S.** 2003: Anthropogenic contributions to atmospheric Hg, Pb and As accumulation recorded by peat cores from southern Greenland and Denmark dated using the ^{14}C 'bomb pulse curve'. *Geochimica et Cosmochimica Acta* 67, 3991–4011.
Shotyk, W., Goodsite, M.E., Roos-Barraclough, F., Givelet, N., Le Roux, G., Weiss, D., Cheburkin, A.K., Knudsen, K., Heinemeier, J., van der Knaap, W.O., Norton, S.A. and **Lohse, C.** 2005: Accumulation rates and predominant atmospheric sources of natural and anthropogenic Hg and Pb on the Faroe Islands. *Geochimica et Cosmochimica Acta* 69, 1–17.

Sigurgeirsson, M.A. 1992: Gjoskumyndanir a Reykjanesi. MSc Thesis, University of Iceland, 113 pp.
Simonarson, L.A. and **Leifsdóttir, O.E.** 2002: Late-Holocene sea-level changes in south and southwest Iceland reconstructed from littoral molluscan stratigraphy. *The Holocene* 12, 149–58.
Sjoberg, L.E., Pan, M., Asenjo, E. and **Erlingsson, S.** 2000: Glacial rebound near Vatnajokull, Iceland, studied by GPS campaigns in 1992 and 1996. *Journal of Geodynamics* 29, 63–70.
Skirnisson, K., Galaktionov, K.V. and **Kozminsky, E.V.** 2004: Factors influencing the distribution of digenetic trematode infections in a mudsnail (*Hydrobia ventrosa*) population inhabiting saltmarsh ponds in Iceland. *Journal of Parasitology* 90, 50–59.
Sveinbjornsdottir, A.E., Eiriksson, J., Geirsdottir, A., Heinemeier, J. and **Rud, N.** 1993: The Fossvogur marine sediments in SW Iceland–confined to the Allerod Younger Dryas transition by AMS C-14 dating. *Boreas* 22, 147–57.
Thirlwall, M.F., Gee, M.A.M., Taylor, R.N. and **Murton, B.J.** 2004: Mantle components in Iceland and adjacent ridges investigated using double-spike Pb isotope ratios. *Geochimica et Cosmochimica Acta* 68, 361–86.
Thordarson, T. and **Höskuldsson, A.** 2002: *Iceland*. Classic Geology in Europe 3. Terra Publishing, 200 pp.
Thors, K. and **Boulton, G.S.** 1991: Deltas, spits and littoral terraces associated with rising sea-level–Late Quaternary examples from Northern Iceland. *Marine Geology* 98, 99–112.
Thors, K. and **Helgadóttir, G.** 1991: Evidence from south west Iceland of low sea level in early Flandrian times. In Maizels, J.K. and Caseldine, C., editors, *Environmental change in Iceland: past and present*. Kluwer Academic Publishers, 93–104.
van de Plassche, O., van der Schrier, G., Weber, S.L., Gehrels, W.R. and **Wright, A.J.** 2003: Sea-level variability in the northwest Atlantic during the past 1500 years: a delayed response to solar forcing? *Geophysical Research Letters* 30, art-1921.
van der Schrier, G., Weber, S.L., Drijfhout, S.S. and **Lowe, J.A.** 2004: Low-frequency Atlantic sea level variability. *Global and Planetary Change* 43, 129–44.
Wastegard, S., Hall, V.A., Hannon, G.E., van den Bogaard, C., Pilcher, J.R., Sigurgeirsson, M.A. and **Hermanns-Audardottir, M.** 2003: Rhyolitic tephra horizons in northwestern Europe and Iceland from the AD 700s–800s: a potential alternative for dating first human impact. *The Holocene* 13, 277–83.
Weiss, D., Shotyk, W., Appleby, P.G., Kramers, J.D. and **Cherburkin, A.K.** 1999: Atmospheric Pb deposition since the Industrial Revolution recorded by five Swiss peat profiles: enrichment factors, fluxes, isotopic composition, and sources. *Environmental Science and Technology* 33, 1340–52.
Woodworth, P.L. 1990: A search for accelerations in records of European mean sea level. *International Journal of Climatology* 10, 129–43.
——— 1999: High waters at Liverpool since 1768: the UK's longest sea level record. *Geophysical Research Letters* 26, 1589–92.
Woodworth, P.L. and **Player, R.** 2003: The Permanent Service for Mean Sea Level: an update to the 21st century. *Journal of Coastal Research* 19, 287–95.
Zielinski, G.A., Mayewski, P.A., Meeker, L.D., Whitlow, S., Twickler, M.S., Morrison, M., Meese, D.A., Gow, A.J. and **Alley, R.B.** 1994: Record of volcanism since 7000 BC from the GISP2 Greenland Ice Core and implications for the volcano-climate system. *Science* 264, 948–52.